CHAPTER 2

SYNTHESIS OF MULTINUCLEAR CARBONYL COMPLEXES SUPPORTED BY A PARA-TERPHENYL DIPHOSPHINE LIGAND

The text for this chapter was reproduced in part from:

Suseno, S.; Horak, K. T.; Day, M. W.; Agapie, T. *Organometallics*, **2013**, *32*, 6883-6886.

Horak, K. T.; Velian, A.; Day, M. W.; Agapie, T. *Chem. Commun.*, **2014**, *50*, 4427-4429.

Horak, K. T.; Lin, S.; Rittle, J.; Agapie, T. *Organometallics*, **2015**, *34*, 4429-4432.

Abstract

Multinuclear hetero- and homometallic clusters supported by *para*-terphenyl diphosphine ligands were targeted with the goal of studying cooperative small molecule activation across multiple metal centers. A series of isostructural trinuclear complexes of metal composition Pd_2Fe, Pd_2Co, and Ni_2Fe, were synthesized in a stepwise fashion. Using dinuclear precursors (Pd^I_2 and Ni^I_2) supported by *para*-terphenyl diphosphine ligands allowed for the selective incorporation of a single additional metal center. The effects of both metal composition and ligand electronics on cluster properties were studied. These results highlight the importance of metal-metal interactions in mixed-metal sites of structurally analogous clusters. Additionally, cofacial Fe_2, Co_2, Ni_2, and Ni_3 complexes supported by a *para*-terphenyl diphosphine ligand were prepared. Central arene deplanarization and a μ_2:(η^3,η^3) coordination mode suggest partial bis-allyl character in the Fe_2 and Co_2 complexes. An oxidation induced shift in Fe_2-arene binding highlights the non-innocent nature of the arene ligand.

INTRODUCTION

Discrete mixed-metal complexes have been studied for molecular-level insight into the structural and electronic factors that influence cluster properties.[1] As the performance of heterogenous catalysts, in terms of activity, durability, selectivity, or cost, can be improved upon inclusion of cometals, an understanding of the underlying metal-metal interactions is needed.[2] To gain insight into such interactions, the study of well-defined, homogeneous, multinuclear heterometallic complexes has been pursued. Heterometallic dinuclear complexes are an active area of current research.[3] Additionally, heterometallic trinuclear complexes in triangular geometries are particularly appealing as one of the simplest model clusters displaying major and minor metal components and direct interactions between all metals, similar to heterogeneous catalysts. Although many advances have been made on the synthesis of multinuclear complexes containing isolated triangular heterometallic motifs,[2, 4] systematic access to related isostructural clusters suitable for structure-property studies is limited. Triangular trinuclear motifs are common in multinuclear heterometallic complexes, but differences in nuclearity, supporting ligands, or cluster oxidation states make systematic comparisons challenging.[2]

Another advantage of multinuclear systems is their potential to facilitate multi-electron transformations by distributing the redox load across several metal centers. Dinuclear metal complexes also have the potential to act in a cooperative fashion in small molecule activation and multi-electron processes.[5] In particular, low-valent Fe_2, Co_2, and Ni_2 complexes have been shown to participate in a variety of transformations, including proton reduction,[5a-c] dihydrogen activation,[5d] Pauson-Khand-type cycloadditions,[5e] C–C coupling,[5f-h] group transfer,[5i, 5j] and carbon dioxide activation.[5k-n]

The development of novel dinucleating ligand scaffolds and complexes capable of both undergoing redox processes and facilitating novel chemical transformations is currently a topic of active research.[6] Our group has recently utilized bis- and tris(phosphinoaryl)benzene ligands as multinucleating scaffolds for Ni and Pd complexes, where the central arene participates as a flexible donor ligand.[5g, 7]

The following chapter summarizes two distinct projects targeting multinuclear hetero- and homometallic complexes. Herein we report the rational synthesis of a series of isostructural, low oxidation state heterometallic complexes of the M_2M'-type, supported by two *para*-terphenyl diphosphine ligands with differing central arene electronics. We also describe a series of homometallic, dinuclear, first-row transition metal complexes supported by a *para*-terphenyl diphosphine and study the flexible Fe_2-arene coordination observed upon one-electron redox chemistry.

RESULTS AND DISCUSSION

2.1 Ligand Synthesis

Scheme 1. Synthesis of ligand *para*-terphenyl diphosphine ligands

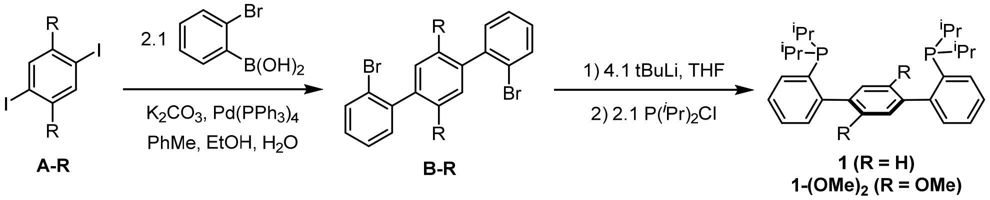

The synthesis of the parent *para*-terphenyl diphosphine ligand (**1**) was accomplished according to literature procedure (Scheme 1).[8] The synthesis of the more electron-rich *para*-terphenyl diphosphine ligand, **1-(OMe)$_2$**, which contains a 1,4-dimethoxybenzene central arene as opposed to a central phenylene, was accomplished using a similar synthetic route (Scheme 1). A Pd-catalyzed Suzuki coupling between 2-bromophenyl boronic acid and 2,5-diiodo-1,4-dimethoxy benzene (**A**) provided the desired *para*-terphenyl dibromide precursor (**B**). Subsequent lithium halogen exchange using *tert*-butyl lithium (*t*BuLi) followed by addition P(*i*Pr)$_2$Cl yielded the desired ligand, **1-(OMe)$_2$**, following workup.

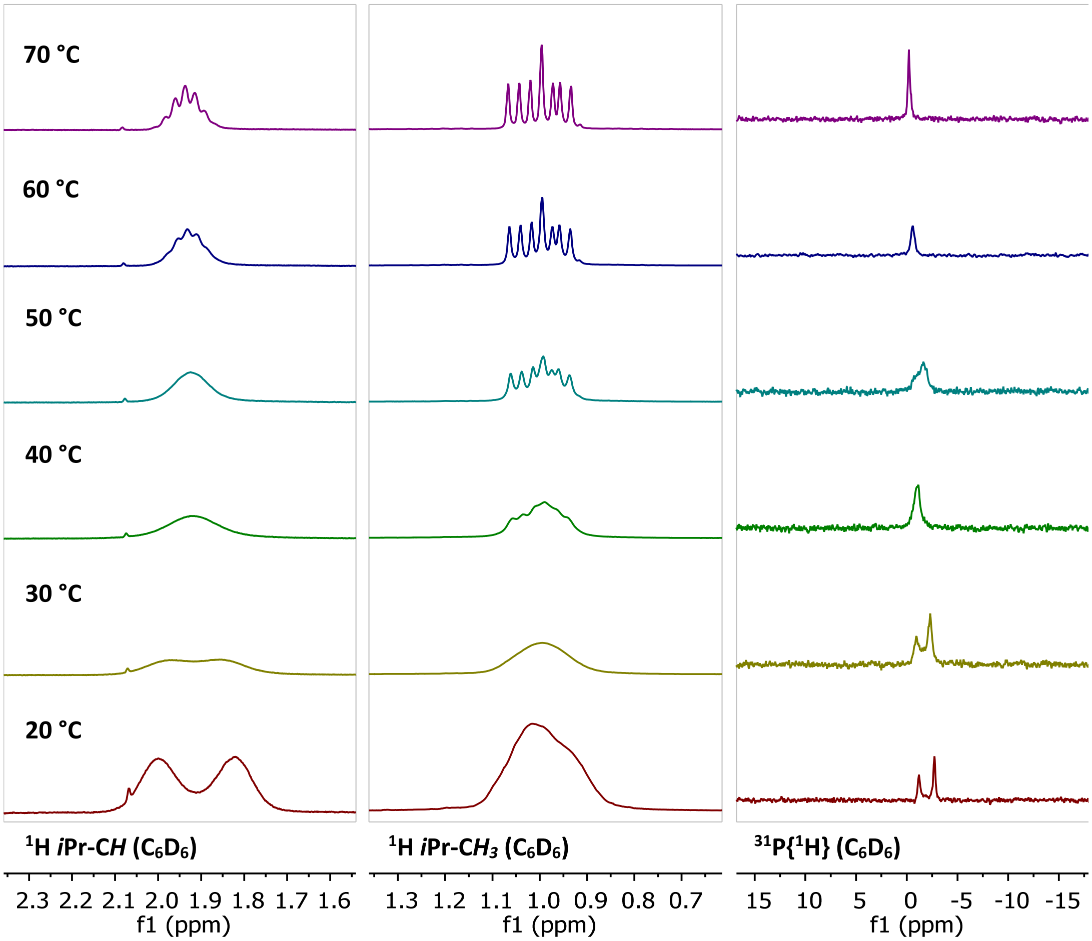

Figure 1. VT-NMR spectra for **1-(OMe)$_2$**.

In solution, **1-(OMe)$_2$** shows two broad *i*Pr methine resonances (2.05, 1.87 ppm) and a broad methyl signal by ^{1}H NMR. Two ^{31}P{^{1}H} signals (-1.18, -2.67 ppm) of inequivalent integration are also observed in contrast to **1**, which shows a single peak at 7.55 ppm (Figure 1). These data are consistent with hindered rotation around the aryl–

aryl bonds at room temperature as a result of the steric clash between the bulky phosphine moieties and the *ortho*-methoxy central arene substituents of **1-(OMe)$_2$**. Similar solution NMR behavior has been reported in a related *meta*-terphenyl diphosphine ligand.[9] To test this hypothesis, variable temperature (VT) NMR experiments were pursued with **1-(OMe)$_2$**. Heating a sample of **1-(OMe)$_2$** to 70 °C in C_6D_6 was sufficient for coalescence of the *i*Pr methine proton resonances and resulted in substantially sharper methyl signals (Figure 1). Additionally, a single ^{31}P resonance at -0.2 ppm was observed at 70 °C, confirming the presence of a single ligand rather that two distinct phosphorus-containing species in solution. The synthesis of **1-(OMe)$_2$** allows for a study of the effects of central arene electronics on the spectroscopic properties of supported metal complexes.

2.2 Synthesis and Characterization of Heterometallic Trinuclear M_2M'-Type Clusters

We have previously reported the chemistry of homometallic clusters coordinated by multidentate phosphinoarene ligands.[7a, 8, 10] Targeting heterometallic trinuclear clusters, dinuclear Pd_2 (**2**) and Ni_2 (**7**) precursors were treated with the tetracarbonyl anions of Fe and Co (Scheme 2). $[Na]_2[Fe(CO)_4]$ was found to react with **2** and **7** to yield $[Pd_2Fe]^0$ (**3**) and $[Ni_2Fe]^0$ (**8**) cores, respectively, while $[Na][Co(CO)_4]$ generated the corresponding $[Pd_2Co]^+$ (**4**) core following reaction with **2**. Reactions of **7** and $[Na][M(CO)_n]$ (M = Co (n = 4), Mn (n = 5)) precursors yielded multinuclear Ni-carbonyl clusters, which will further discussed in Section 2.3, rather than a $[Ni_2M]^+$ (M = Co, Mn) core. $Mo(CO)_3(MeCN)_3$ was found to react with **2** to yield the corresponding $[Pd_2Mo]^{2+}$ core (**6**), demonstrating that salt metathesis reactions with anionic transition metal carbonyl precursors were not required to construct heterometallic trinuclear complexes.

Scheme 2. Synthesis of heterometallic trinuclear complexes.

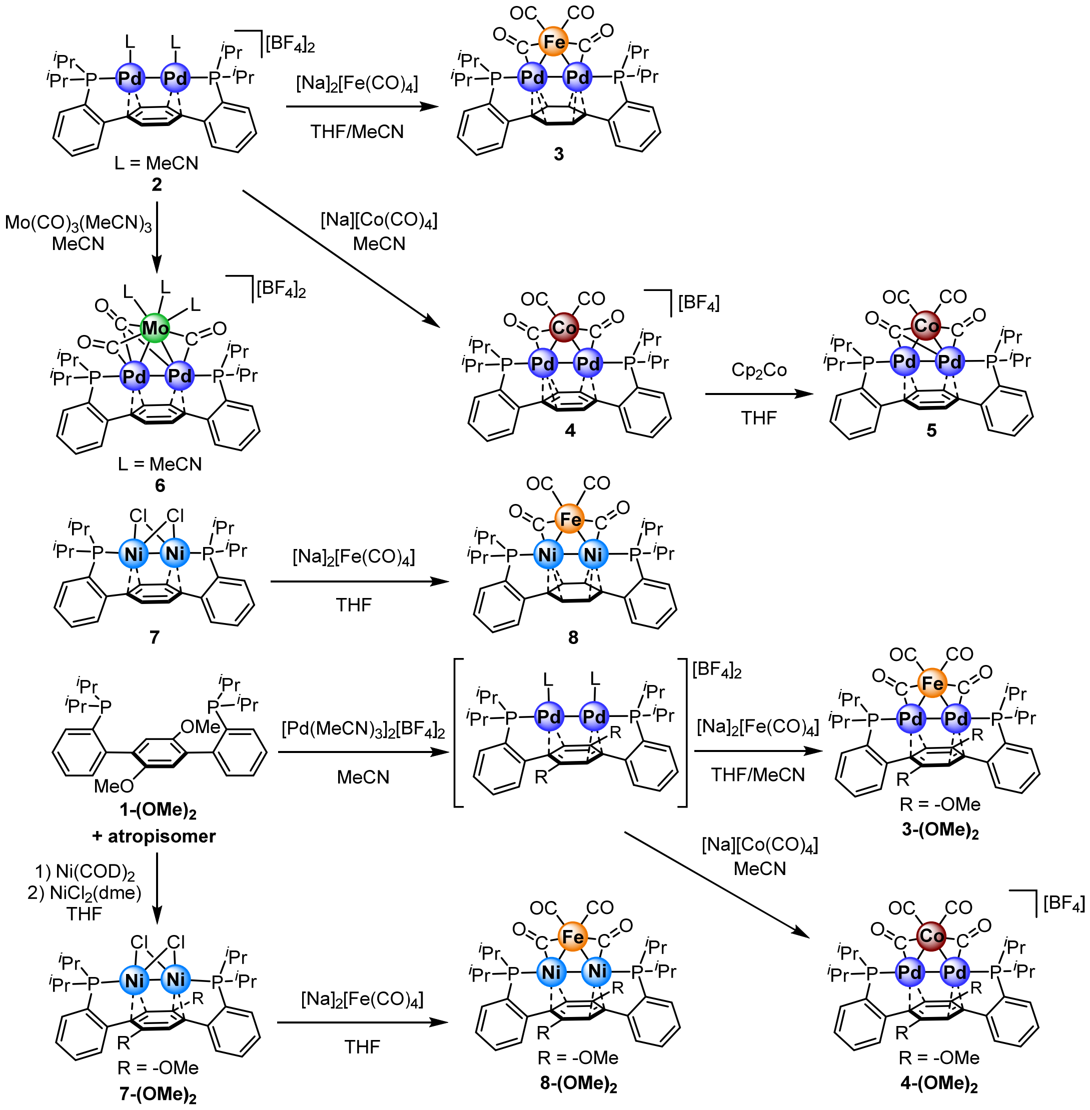

These complexes represent very rare examples of triangular clusters, with only two Pd_2Co, four Ni_2Fe, and no Pd_2Fe species structurally characterized previously.[4a, 4b, 4e-g, 4i] Spectroscopic and structural parameters of these reported clusters are challenging to compare due to differences in cluster oxidation state and the identity of supporting ligands. The present series maintains the same ligand environment while varying the identity of the major and minor metal components. To analyze the effect of ligand electronics on cluster properties, a diphosphine variant with *para*-methoxy-substitution of the central arene, **1-(OMe)$_2$** (Scheme 2), was employed to support analogous multinuclear complexes. A one-pot metalation of **1-(OMe)$_2$** with $[Pd_2(MeCN)_6][BF_4]_2$ followed by the addition of $[Na]_2[Fe(CO)_4]$ or $[Na][Co(CO)_4]$ yielded the desired $[Pd_2Fe]^0$ (**3-(OMe)$_2$**) or $[Pd_2Co]^+$ (**4-(OMe)$_2$**) cores, respectively. Adapted literature procedures were used to synthesize the analogous Ni_2 precursor (**7-(OMe)$_2$**) via a comproportionation reaction with $Ni(COD)_2$ (COD = 1,5-cyclooctadiene) and $NiCl_2$dme (dme = 1,2-dimethoxyethane). **7-(OMe)$_2$** was allowed to react with $[Na]_2[Fe(CO)_4]$ to obtain the targeted $[Ni_2Fe]^0$ core (**8-(OMe)$_2$**). Multiple techniques have been utilized to compare the reported compounds: electrochemical measurements, NMR spectroscopy, Mössbauer spectroscopy, and IR spectroscopy in addition to structural comparisons from solid-state structures.

Single crystal X-ray diffraction (XRD) studies were performed for **3**, **4**, **6**, **3-(OMe)$_2$**, and **8** (Figure 2). The homodinuclear moiety (M_2) is bound to the phosphine and arene donors in a manner reminiscent of the precursors (**2** and **7**).[8, 10a, 11] The apical metal (M') of the $M_2M'(CO)_4$–type clusters display interactions with the M_2 core and two CO ligands, one bridging each M–M' interaction. For complex **6**, the all three CO ligands support the Pd_2 core-Mo interaction. One CO ligand bridges across one face of the Pd_2Mo core in a μ_3 fashion, while the remaining two each bridge a different Pd–Mo interaction. Despite the variation of apical and dinuclear core metal identity as well as ligand electronics, the clusters remain largely isostructural, with the exception of **6**. The metal-metal distances for $Pd_2M(CO)_4$–type clusters are similar between complexes **3**, **4**, and **3-(OMe)$_2$** with Pd–Pd distances ranging between 2.5643(3) and 2.5853(3)(2) Å and Pd–M' distances ranging between 2.5374(3) and 2.5541(6) Å. Owing the larger size of Mo compared to Fe or Co, complex **6** shows a considerably expanded trinuclear core with a Pd–Pd distance 2.6220(2) Å and Pd–Mo distances of 2.8176(3) and 2.7516(3) Å. Complex **8** shows shorter metal-metal distances of 2.3931(8) and 2.4169(6) Å for Ni–Ni and Ni–Fe, respectively, due to the smaller size of Ni compared to Pd. Both average Pd–Pd and Ni–Ni distances are similar to the metal-metal distances in a previously reported mono-atom bridged complexes such as the dmdbt-Pd_2 complex (dmdbt = 4,6-dimethyldibenzothiophene) and complex **7**.[8, 10a]

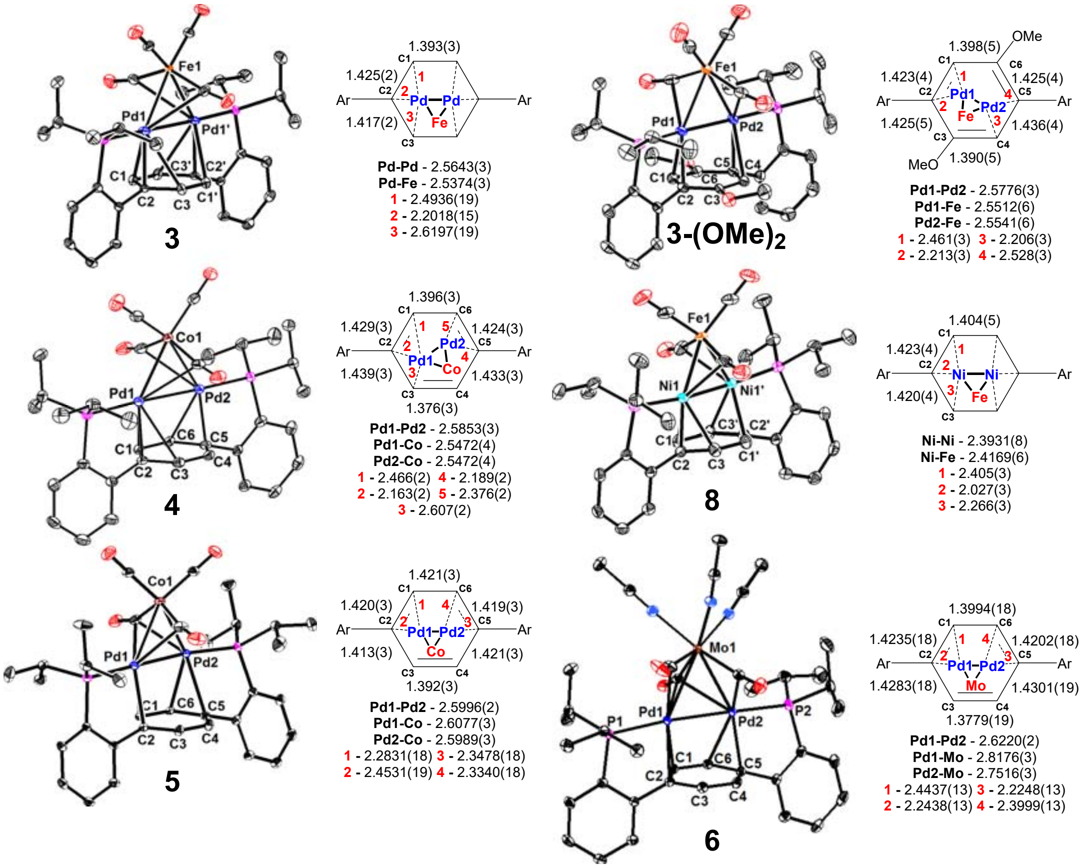

Figure 2. Solid-state structures and select bond metrics for the synthesized trinuclear compounds. Hydrogen atoms, solvent, and counter ions have been omitted for clarity.

The binding mode of the central arene and the NMR characteristics core for each complex allows for the interrogation of the effect of changing of the apical metal on the M_2 moiety. Isoelectronic compounds **3** and **4** show slightly different metal-arene interactions, changing from *pseudo-*C_2 μ_2:(η^3,η^3) to μ_2:(η^3,η^2). The closest Pd–C contacts are slightly shorter in **4** compared to **3**, potentially a consequence of the cationic nature of **4** leading to stronger metal-arene interactions. Complex **6** and **3-(OMe)$_2$** both show different μ_2:(η^2,η^2) coordination modes in the solid-state with the M_2 moiety of the former binding to C1–C2 and C4–C5 while the latter coordinates to adjacent C–C bonds (C1–C2 and C5–C6) as seen in the Pd_2 precursor **2**. Complex **8** shows a *pseudo-*C_2 μ_2:(η^3,η^3) coordination mode reminiscent of **3**. In solution, complexes **3**, **4**, and **8** show single resonances (^{1}H NMR spectroscopy) for central arene protons (δ(ppm) **3**: 5.92; **4**: 6.39; **8**: 5.78), indicating fluxional central arene coordination on the NMR timescale. The significantly upfield shifted resonance for the central arene protons compared to **1** (7.55 ppm) is indicative of metal-arene interactions as observed by XRD. NMR data for the $M_2M'(CO)_4$-type clusters supported by **1-(OMe)$_2$** ligand also show an upfield shift of the central arene proton resonance (δ(ppm) **3-(OMe)$_2$**: 5.51; **4-(OMe)$_2$**: 5.80; **8-(OMe)$_2$**: 5.30) compared to free ligand (6.83 ppm) again consistent with strong metal-arene interactions. Distortions of the central arene consistent with a reduced arene or bis-allyl assignment as seen in previously characterized Co_2 and Fe_2 complexes, which will be discussed in greater detail in Section 2.3, are not consistent with the solid-state structures despite spectroscopic evidence for significant metal-arene interactions.[10c]

Solution infrared (IR) spectroscopy was used as a measure of the effect of the identity of the homodinuclear component (M_2) and supporting ligand on the cluster properties. The clusters containing the $Fe(CO)_4$ moiety display bands corresponding to C–O stretches (ν_{CO}(cm^{-1}) **3**: 1901 (s), 1874 (m), 1848 (s), 1843 (w, sh); **3-(OMe)$_2$**: 1898 (s), 1867 (m), 1838 (s, coincidental overlap with weak shoulder ν_{CO} stretch); **8**: 1896 (s), 1874 (m), 1821 (m), 1798 (w, sh)). Complex **8** shows a larger reduction in average carbonyl stretching frequency (20 cm^{-1}).

The effect of the more electron-rich central arene of **3-(OMe)$_2$** is seen in the average carbonyl stretching frequencies that shift by 7 cm^{-1} to lower energy compared to **3**, though the magnitude of the change is smaller. These differences indicate that the moiety in direct contact with Fe (Ni$_2$ or Pd$_2$) has a larger effect than the more distant arene ligand. Mössbauer data was obtained to further to probe the electronic differences between Fe-containing complexes (Figure 3-5). The isomer shifts and quadrupole splitting of all complexes (δ (mm s^{-1}) (ΔEq (mm·s^{-1})) **3**: -0.10 (1.08), **3-(OMe)$_2$**: -0.09 (1.13), **8**: -0.11 (0.83)) are within 0.02 mm s^{-1} range suggesting the presence of similar Fe centers despite the differences observed by IR spectroscopy. Complex **4** shows IR absorptions at higher energy (2057 (s), 2012 (m), 1915 (m), and 1878 (w, sh) cm^{-1}) compared to **2**, consistent with the expected trends for isoelectronic complexes based on higher nuclear charge for Co vs Fe. Complex **6** shows three IR absorptions (1900 (s), 1847 (s), and 1799 (s) cm^{-1}) consistent with the asymmetry of the solid-state structure. The C_{3v} symmetry of the Mo(CO)$_3$(MeCN)$_3$ precursor results in the appearance of only two IR absorptions: an A$_1$ set at 1920 cm^{-1} and an E set at 1796 cm^{-1}.[12] The average ν_{CO} stretching frequencies of complex **6** (1849 cm^{-1}) are slightly shifted to higher energy compared to the precursor (1837 cm^{-1}), consistent with binding of the Mo center to an electron-deficient dicationic Pd$_2$ core.

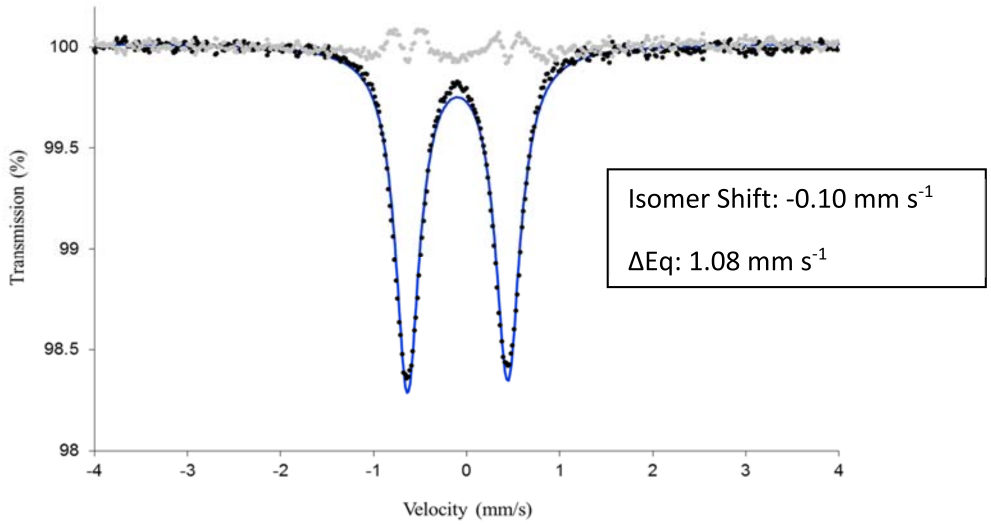

Figure 3. Zero-field ^{57}Fe Mössbauer spectrum for **3**, 80 K. Data: black dots; spectral fit: blue line; and residual: grey dots.

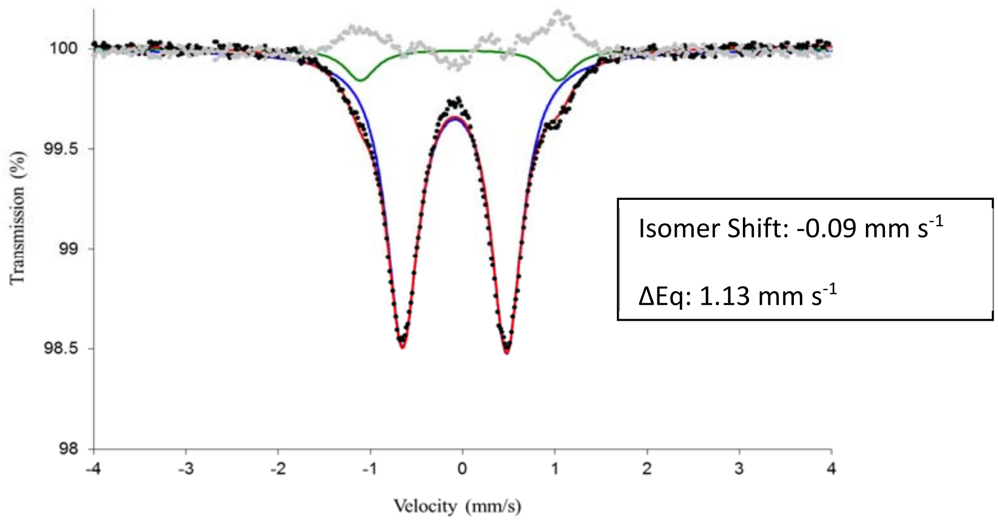

Figure 4. Zero-field ^{57}Fe Mössbauer spectrum for **3-(OMe)$_2$** and minor decomposition (green line) following removal from glovebox, 80 K. Data: black dots; spectral fit: red line; deconvolution: blue and green lines; residual: grey dots.

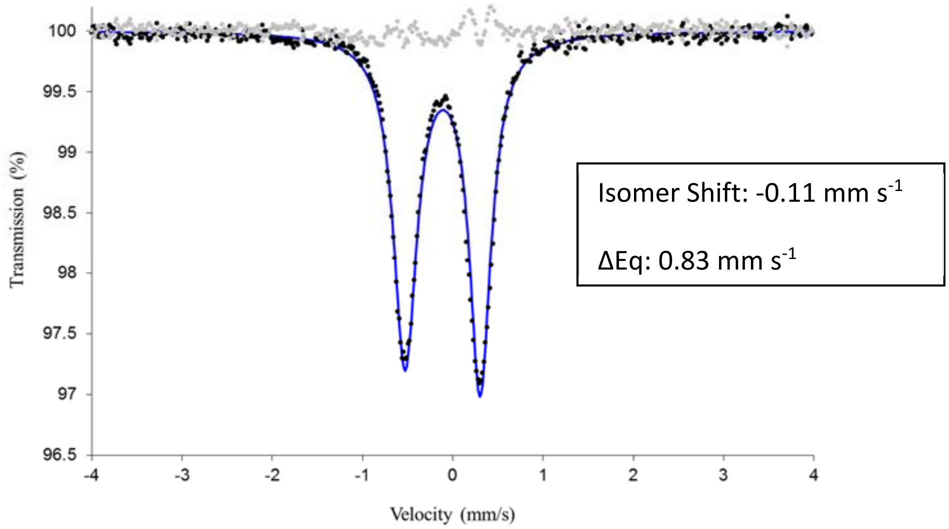

Figure 5. Zero-field ^{57}Fe Mössbauer spectrum for **8**, 80 K. Data: black dots; spectral fit: blue line; and residual: grey dots.

Computational studies were performed on simplified models of **3**, **4**, **3-(OMe)$_2$**, and **8** (see Table 3 for details and representative molecular orbitals for all compounds). Calculated metal-metal distances are in good agreement with solid-state parameters obtained from XRD studies (Table 1) with largest deviations in M–M and M–M' distances see for complex **7** at 0.046 and 0.020 Å, respectively. Differences in computed average carbonyl stretching frequencies largely agree with the experimental differences (Table 2). Select computed MOs are highlighted for a truncated model of **3** (**3-Me$_2$**) (Figure 3). Natural bond orbital (NBO) calculations reveal Wiberg bond indices (WBIs) consistent with weak bonds of comparable strength for both M–M (**3-Me$_2$**: 0.1647, **4-Me$_2$**: 0.1647, **3-(OMe)$_2$-Me$_2$**: 0.1658, **8-Me$_2$**: 0.1647) and M–M' (**3-Me$_2$**: 0.2147, **4-Me$_2$**: (0.1758, 0.1753), **3-(OMe)$_2$ -Me$_2$**: (0.2133, 0.2131), **8-Me$_2$**: 0.2140) interactions in all complexes (Figure 27). These results are consistent with a previously reported bonding picture with the formally 18-electron M(CO)$_4$ fragment donating electron density to the M$_2$ fragment, which states that M–M' interactions provide the largest stabilization responsible for cluster formation.[13] These weak M–M' interactions suggest direct electronic communication between the M(CO)$_4$ moiety and the homodinuclear core.

Table 1. Comparison of Calculated and Experimental Bond Metrics

Complex	**ν_{CO}(calc) (cm^{-1})**	**Average ν_{CO}(calc) (cm^{-1})**	**ν_{CO}(expt) (cm^{-1})**	**Average ν_{CO}(expt) (cm^{-1})**
3	2029.2, 1980.3, 1948.4, 1927.5	1971.4	1901 (s), 1874 (m), 1848 (s), 1843 (w, sh)	1867
4	2110.7, 2076.0, 2023.8, 1991.2	2050.4	2057 (s), 2012 (m), 1915 (m), 1878 (w, sh)	1966
3-(OMe)$_2$	2024.3, 1976.3, 1931.4, 1909.3	1960.3	1898 (s), 1867 (m) 1838 (s, coincidental overlap with weak should stretch)	1860
8	2015.0, 1964.1, 1924.7, 1902.8	1951.7	1896 (s), 1874 (m) 1821 (m), 1798 (w, sh)	1847

Table 2. Comparison of Calculated and Experimental IR Parameters

Complex	**d(M-M)$_{calc}$ (Å)**	**d(M-M)$_{expt}$ (Å)**	**d(M-M')$_{calc}$ (Å)**	**d(M-M')$_{expt}$ (Å)**
3	2.5889	2.5643(3)	2.5379, 2.5382	2.5374(3)
4	2.5983	2.5853(3)	2.5463, 2.5464	2.6077(3), 2.5472(4)
3-(OMe)$_2$	2.5988	2.5776(3)	2.5398, 2.5402	2.5512(6), 2.5541(6)
8	2.3474	2.3931(8)	2.3970, 2.3976	2.4169(6)

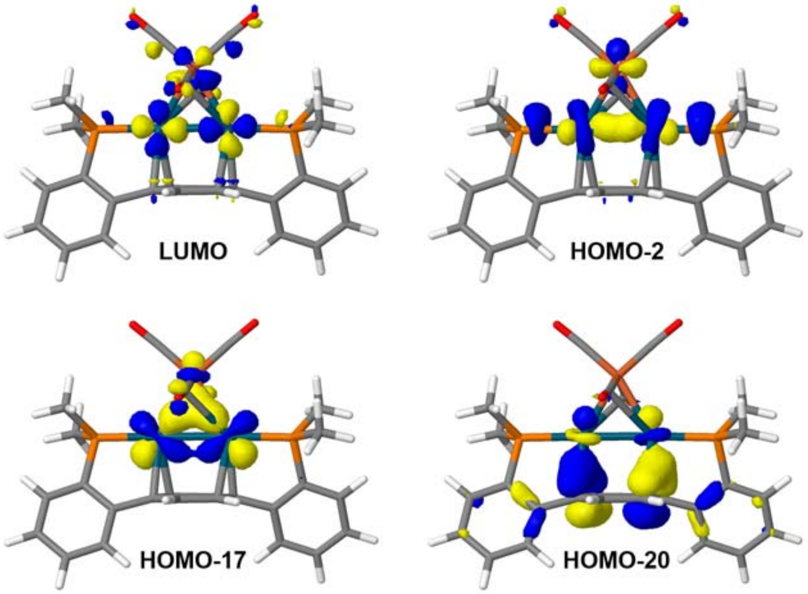

Figure 6. Select molecular orbitals calculated for a truncated version of **3** (**3-Me$_2$**) that show interactions between (clockwise from LUMO), M–M/M–M', M–M, M–arene, and M–M' moieties.

Cyclic voltammetry (CV) experiments were conducted on complexes of the trinuclear series (see Experimental Section for full conditions). Quasireversible reductions for all complexes were observed at (**3**: -2.43 V), (**4**: -1.31, -1.81 V), (**3-(OMe)$_2$**: -2.62 V), and (**8**: -2.29, -2.75 V) vs the ferrocene/ferrocenium (Fc/Fc$^+$) couple in tetrahydrofuran (THF) (Figure 7). Irreversible oxidations are observed for all complexes. While comparable CV data for Pd_2Fe and Ni_2Fe complexes are absent from the literature to the best of our knowledge, a systematic study of ligand variation in isoelectronic Pd_2Co complexes has been reported.[4g] The reported trinuclear complex $[Pd_2Co(\mu\text{-dppm})_2(\mu_3\text{-CO})_2(CO)_2][PF_6]$ (dppm = 1,1-bis(diphenylphosphino)methane) was reported to have two one-electron reductions with $E_{1/2}$ potentials comparable to **4** at -1.20 V and -1.63 V vs Fc/Fc$^+$ in THF despite significant differences in supporting ligands.

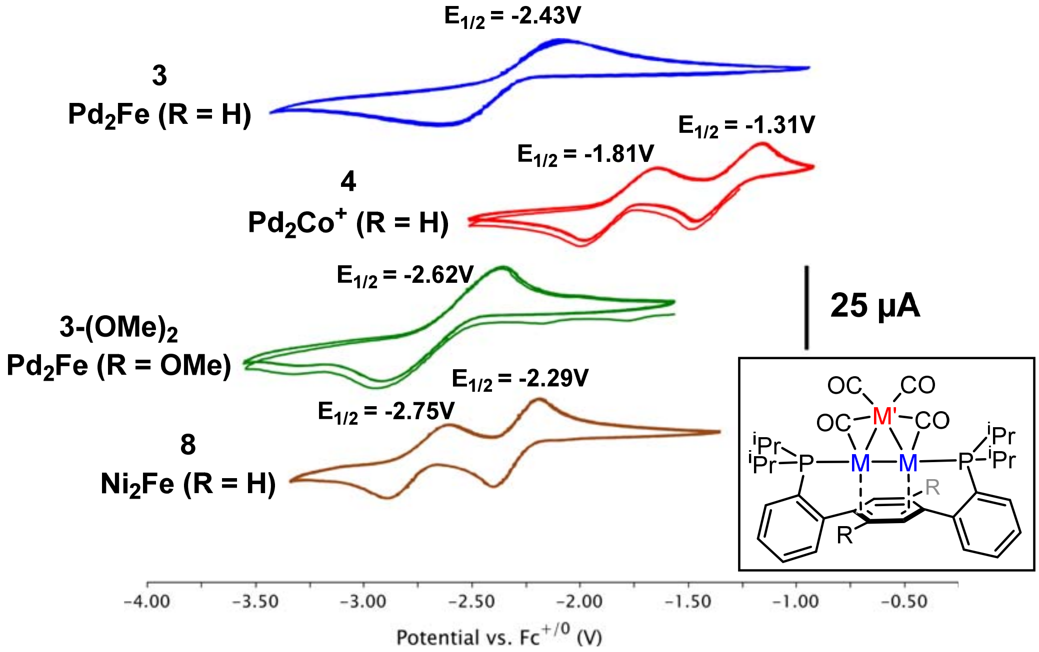

Figure 7. Cyclic voltammetry data for the reported $M_2M'(CO)_4$–type complexes.

Both Pd_2Fe complexes, **3** and **3-(OMe)**$_2$, display CV behavior with only a single, two-electron electrochemical reduction observed at more negative potentials than both peaks for **4**. The reduction of **3-(OMe)**$_2$ is ~200 mV more negative than **3**, a consequence of the more electron-rich supporting arene. The Ni_2Fe complex **8** shows similar electrochemical behavior as **4**, with two reduction events, but at potentials ~1 V more negative. The more electron-rich Ni_2Fe complex, **8-(OMe)**$_2$, also shows two quasireversible reductions (-2.42, -2.88 V) shifted to more negative potentials by approximately ~130 mV compared to **8** (Figure 8). The increased charge of the Pd_2Co core relative to the Ni_2Fe or Pd_2Fe complexes likely contributes to the positive shift in the redox events for complex **4**, making the reduction more facile. Overall, the electrochemical data indicate that metal composition and supporting ligand play a significant role in cluster properties as the variation of apical metal (Fe to Co) and dinuclear core (Pd_2 to Ni_2) significantly affects redox behavior.

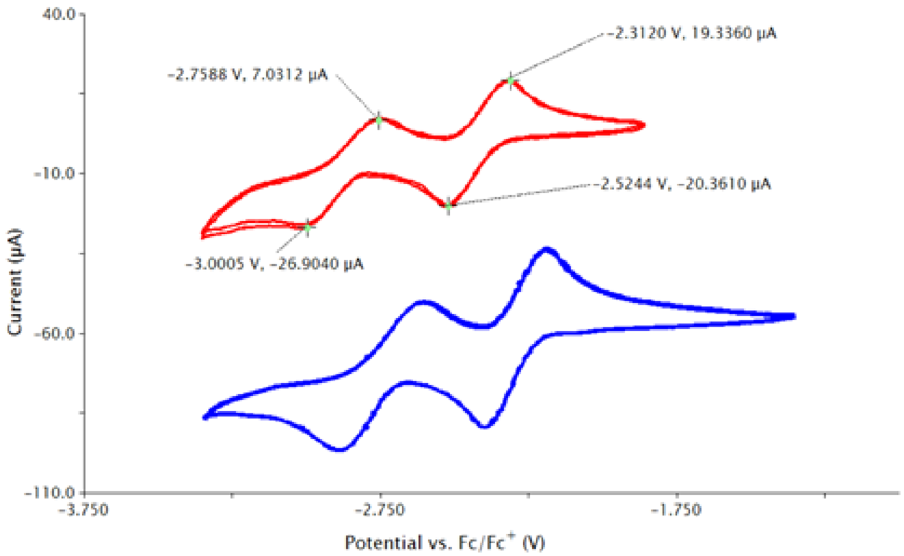

Figure 8. A comparison of cyclic voltammetry data for complexes **8** and **8-(OMe)$_2$**.

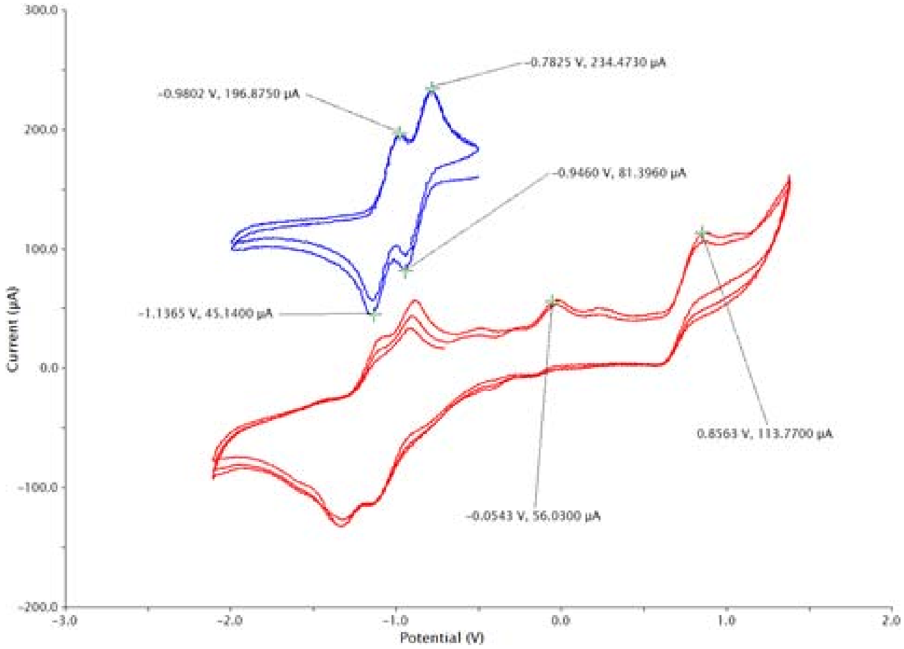

Figure 9. Cyclic voltammetry data for the complex **6**.

CV experiments in acetonitrile (MeCN) were also conducted on complex **6** (Figure 9). As with the aforementioned trinuclear clusters, irreversible oxidations are observed. Reminiscent of the electrochemical behavior of **4** and **8**, a pair of quasireversible reduction events (-0.64,

-1.28 V) are observed for complex **6**. These reductions occur at considerably more positive potentials compared to $M_2M'(CO)_4$-type clusters, which is likely attributable to the increased cationic charge of compound **6**.

In light of the electrochemical observations, chemical reductions were performed with **3**, **4**, **3-(OMe)$_2$**, and **8**. The Fe-containing complexes led to complex mixtures of products. The neutral $[Pd_2Co]^0$ core, complex **5**, was successfully isolated upon treatment of **4** with one equivalent of cobaltocene (Scheme 2). While unstable at room temperature, single crystals suitable for XRD analysis were obtained at -35 °C (Figure 2). Coordination of the dinuclear core to the central arene has shifted to μ_2:(η^2,η^2) and the bridging CO ligands have adopted a different geometry, with one bound μ_3 across the Pd_2Co core, indicative of increased back-bonding to the π-acidic ligands. In agreement, IR spectra of complex **5** display CO stretching frequencies of 2007 (s), 1920 (m, sh), 1879 (m), and 1837 (m) cm^{-1} that are shifted to lower energy compared to **4**. Increases in Pd–Co and Pd–Pd bond distances by 0.06 and 0.03 Å, respectively, are consistent with weakened M–M and M–M' interactions. Solution electron paramagnetic resonance (EPR) data for **5** obtained in a toluene glass at 77 K shows a rhombic signal (g = 2.128, 2.032, 1.930) with hyperfine coupling to the Co nucleus (A = 119, 65, 105) (Figure 10), and compares well to a comparable literature complex.[4g] The flexible coordination the central arene and CO ligands likely helps stabilize complex **5**, allowing for its isolation. Overall, the synthesis of a new series of heterometallic trinuclear complexes allowed for the systematic study of the effects of changes in metal composition and ligand electronics.

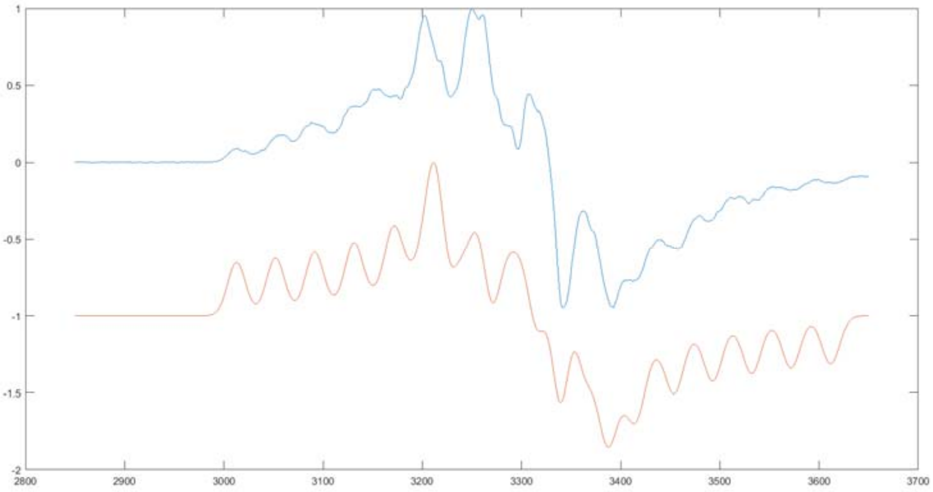

Figure 10. X-band EPR spectrum of **5** collected at 77K in a toluene glass (blue). EasySpin simulation of EPR data (red).

2.3 Synthesis and Characterization of Homometallic Di- and Trinuclear Carbonyl Complexes

Efforts targeting homometallic multinuclear complexes were also pursued. After multiple days of ultraviolet irradiation, a THF solution of compound **1** and $Fe_3(CO)_{12}$ yielded a Fe_2 complex, **9**, in 11% isolated yield (Scheme 3). Refluxing a toluene (PhMe) solution of compound **1** and $Co_2(CO)_8$ at 110 °C overnight cleanly afforded a Co_2 complex, **11**, in 54% isolated yield (Scheme 3). The analogous cofacial Ni_2 complex was prepared by the reduction of a previously synthesized Ni^I–Ni^I dichloride complex, **7**,[5g] with [Na][Co(CO)$_4$], or [Na][Mn(CO)$_5$] which served as a source of both reducing equivalents and carbon monoxide (CO) ligands. The Ni_2 complex, **12**, was isolated in 11% yield (Scheme 1). An alternative synthesis of complex **4** involved the careful addition of four equivalents of CO to two equivalents of Ni(COD)$_2$ and compound **1** (Scheme 3). However, this method was lower yielding and not used as the primary synthetic route. The low yields for compounds **9** and **12** are due to purification procedures, which require isolation of crystalline material. The reaction mixtures for the syntheses of these complexes display the desired compounds as the major species by ^{31}P NMR spectroscopy. An added complication was the gradual conversion of **12** into a mixture of a $Ni_3(CO)_4$ complex (**13-CO**) and a mononickel carbonyl complex (**1-Ni(CO)**) in solution. **13-CO** could be independently synthesized by metalating **1** with three equivalents of $Ni(COD)_2$ in the presence of a five equivalents of carbon monoxide, which afforded the product in 74% yield (Scheme 3). Control of CO stoichiometry is necessary, as a large excess results in the excessive coordination of carbon monoxide to generate previously characterized transfacial dinuclear $Ni(CO)_n$ (n = 2-3) complexes.[8]

Scheme 3. Synthesis of homometallic multinuclear carbonyl complexes of Fe, Co, and Ni

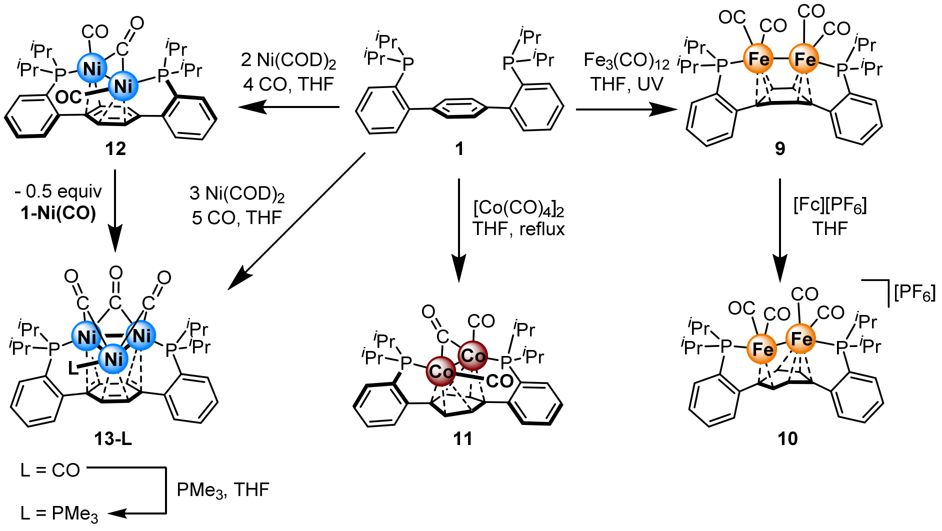

Single crystal XRD studies of complexes **9**, **11**, **12**, and **13-CO** confirmed the stabilization of multinuclear homometallic fragments by metal-arene interactions (Figure 11). The dinuclear core of complex **9** and **11** coordinate in a μ_2:(η^3,η^3) fashion to the central arene. In **9**, the phosphines coordinated to each Fe center are roughly colinear with the Fe–Fe vector, resulting in a structure of *pseudo-*C_{2v} symmetry. The zig-zag arrangement of the P_2Co_2 moiety in **11**, imposed by the bridging and terminal CO ligands on Co, effects the overall *pseudo-*C_2 symmetry of the dicobalt complex. In complex **9**, the planes defined by C1-C2-C3 and C4-C5-C6 show an average dihedral angle of 26° with the C1-C3-C4-C6 plane. Central arene deplanarization is also observed in complex **11**, with a dihedral angle averaging approximately 23° between both the C2-C3-C4 and C5-C6-C1 planes with the C1-C2-C4-C5 plane. The deplanarized central arene carbons of complex **11** are *ortho* to the aryl substituents, oriented to match the Co–Co vector. The C–C bonds separating the η^3-M moieties are considerably elongated, averaging approximately 1.469 Å for C1–C6 and C3–C4 in complex **2** and 1.470 Å for C1–C2 and C4–C5 in complex **11**. These structural features are consistent with reduction of the arene to generate a bis-allyl motif and formal oxidation of the M_2 core by two electrons to yield a M^I–M^I unit (M = Fe, Co). Further supporting this assignment are short M–arene distances that are consistent with literature bisallyl Fe_2 or Co_2 complexes.[14] Bridging arene complexes of Fe_2 and Co_2 displaying a bis-allyl motif are very rare and typically have the two metal centers bound in transfacial manner.[15, 16] Compounds **9** and **11** represent unusual examples of cofacially coordinated μ_2-arene complexes. The Fe–Fe distance in complex **9** (2.7563(2) Å) is comparable to a cofacial μ_2:(η^3,η^3)-toluene Fe_2 complex at 2.746(1) Å,[15b] but shorter than typical bis-allyl diiron compounds which range between 2.927(3) and 3.138(3) Å.[14b-d] The Co–Co distance (2.6035(2) Å) in **11** is in the range for a formal single Co^0-Co^0 bond.[17]

In contrast to the Fe_2 and Co_2 systems, the Ni_2 core of complex **12** binds μ_2:(η^2,η^2) to adjacent C–C bonds of the central arene (Figure 11). In the solid-state, complex **12** shows partial localization of single bond character at C1–C6, C2–C3, and C4–C5, indicative of disrupted aromaticity. No deplanarization of the central arene ligand is observed, suggesting that bisallyl character is not present. While transfacial μ_2:(η^2,η^2)-arene Ni^0Ni^0 complexes are known,[18] complex **12** displays the first structurally characterized cofacial μ_2:(η^2,η^2) binding mode. The coordination sphere of Ni in complex **12** is reminiscent of $Ni_2(CO)_3(dppm)_2$ with a phosphine donor replaced by an arene double bond for each metal center and twisting of the dihedral angle defined by the two terminal carbonyl carbons and the Ni–Ni vector (dppm = bis(diphenyphosphino)methane).[10a]

An XRD study reveals that complex **13-CO** has similar structural features another previously reported trinickel complex supported by a related ligand scaffold (Figure 11).[7a] Instead of a third phosphine arm, Ni3 binds a terminal CO ligand. The Ni_3 core of complex **13-CO** binds μ_3:(η^2,η^2,η^2) to adjacent C–C bonds of the central arene. Central arene C–C bond distances range between 1.419(2) and 1.435(2) Å indicating strong Ni backbonding. This is also corroborated by short Ni-arene distances in **13-CO** which range between 2.130(2) to 2.185(2) Å with an average distance (2.157 Å) comparable to that of **12** (2.195 Å). The Ni–Ni distances in compound **13-CO** (2.4394(3), 2.4466(3), 2.4746(3) Å) are substantially shorter than those in **12** (2.6313(4) Å), which may be attributable to the more constrained triangular geometry. Consistent with the solid-state structure, the solution IR spectrum of **13-CO** shows bands at 2002, 1873, and 1830 cm^{-1}, indicative of terminal and bridging carbon monoxide coordination.[19]

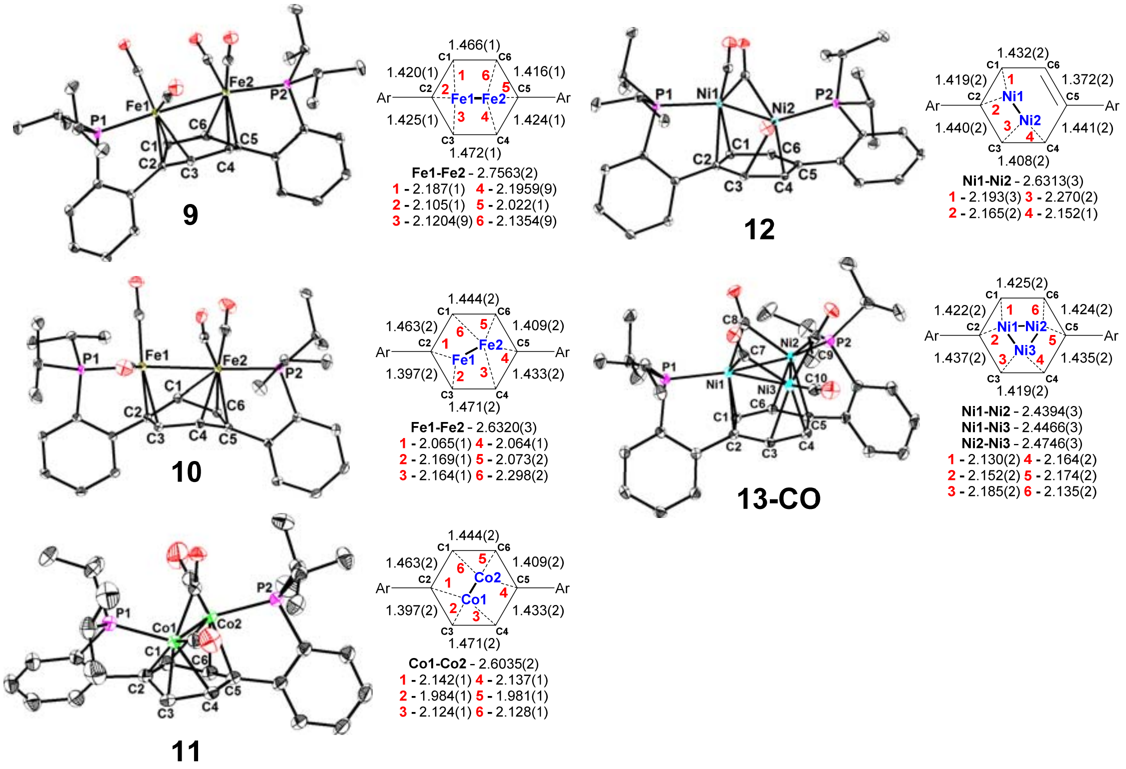

Figure 11. Solid-state structures and select bond metrics for synthesized compounds. Hydrogen atoms, solvent, and counter ions have been omitted for clarity.

The ^{1}H NMR chemical shifts of the central arene protons of complex **9**, **11**, and **12** are shifted upfield in comparison to the parent ligand, as a singlet at 4.39 ppm, a pair of 1:1 singlets at 4.29 and 3.95 ppm, and a singlet at 5.85 ppm, respectively, indicating that strong metal-arene interactions and disruption of aromaticity are preserved in solution. The NMR spectra of **9** are consistent with the high symmetry observed in the solid-state structure. Variable temperature (VT) NMR experiments were performed for complexes **11** and **12**. For **11**, VT ^{1}H NMR experiments show broadening of the central arene and methine protons upon heating, with coalescence observed around 80 °C (Figure 12). At 100 °C, the central arene and methine protons each show a single broad peak. The fluxional process consistent with the observed NMR features involves the interconversion of the two *pseudo*-C_2 isomers by partial rotation of the Co_2 unit around the central arene ring. VT ^{1}H NMR studies with complex **12** show decoalescence of the central arene protons into a pair of doublets at -20 °C (Figure 13). Further cooling to -78 °C was not sufficient to resolve the central arene protons into four separate resonances, indicating that the complex was not locked out as the C_1 solid-state structure due to partial rotation of Ni_2-unit. In agreement, the ^{31}P NMR spectrum shows a single peak, even at -78 °C. The lower energetic barrier for the fluxional process in **12** versus **11** may be due to a smaller molecular distortion, particularly of the central ring, necessary for partial rotation of the M_2 unit of **12**.

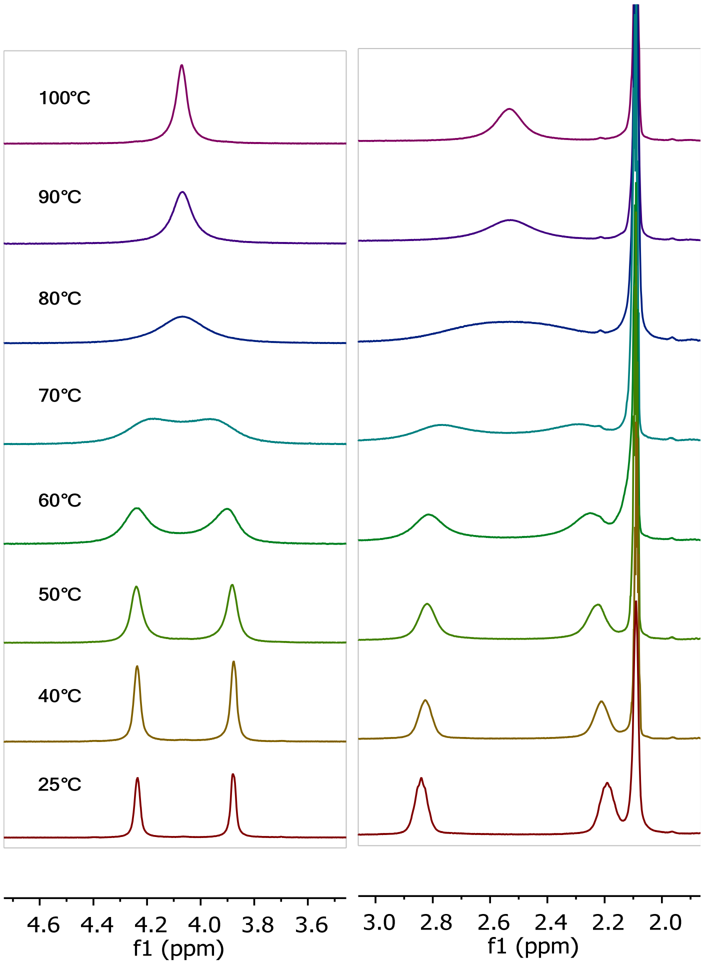

Figure 12. VT ^{1}H NMR (500 MHz, d_8-PhMe) spectra of **11** with central arene protons (Left) and methine protons (Right) shown.

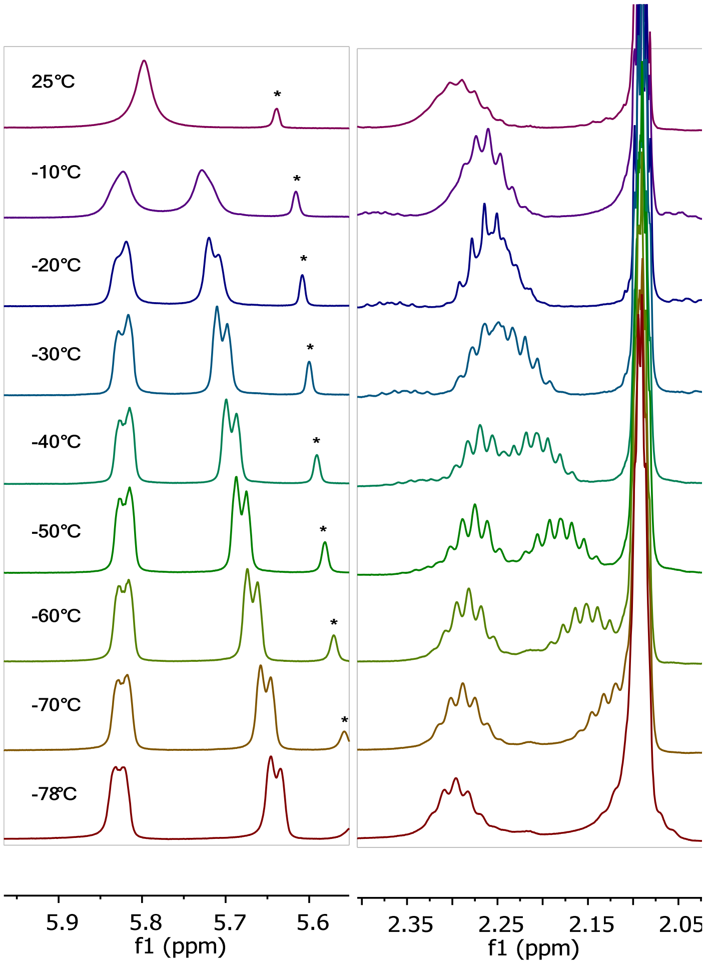

Figure 13. VT ^{1}H NMR (500 MHz, d_8-PhMe) spectra of **12** with central arene protons (Left) and methine protons (Right) shown. Starred peak corresponds to the partial decomposition of **12** to **13-CO** over course of experiment.

The weaker M-arene interactions of **12** compared to **9** or **11** may also contribute to the solution instability of the complex. The disproportionation of the Ni^0 centers and CO ligands of **12** may occur through a bimolecular process. A preliminary XRD structure containing two cocrystallized Ni complexes, one containing a Ni$_3$ core (molecule 1) reminiscent of **13-CO** while the other possesses a Ni(CO)$_2$ unit (molecule 2), which supports this hypothesis (Figure 14). The nickel center of molecule 2 is coordinated by only one phosphine donor, allowing the other to bind to molecule 1. While other disproportionation pathways may also be operative, this structure provides evidence that two equivalents of **12** could exchange a nickel center via a transient dimer complex.

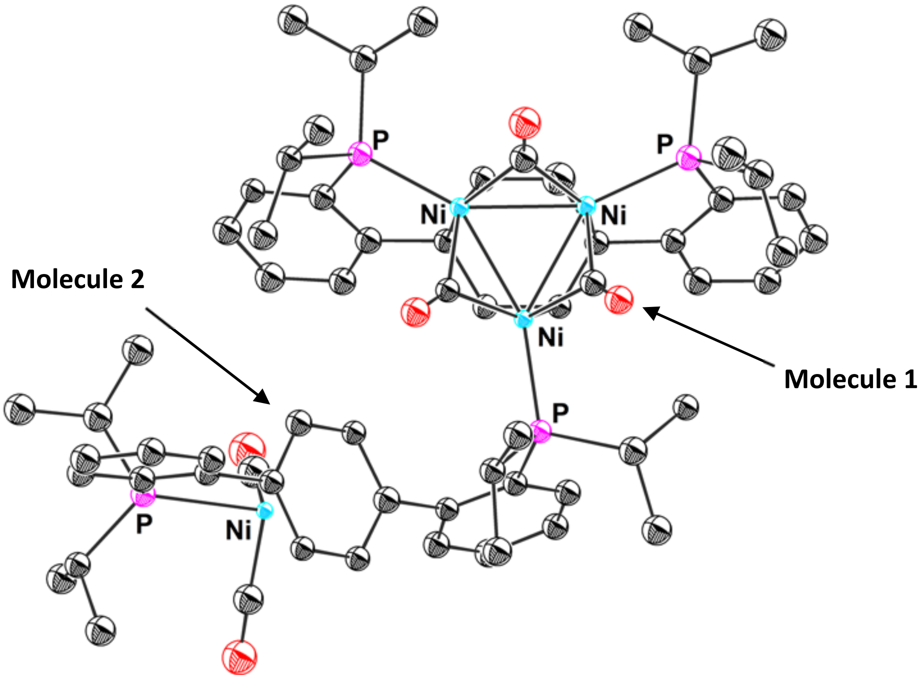

Figure 14. Preliminary solid-state structure highlighting a potential intermolecular pathway for the disproportionation of **12** to **13-CO** and a mononuclear Ni carbonyl complex in solution.

Solution NMR data for **13-CO** is consistent with the *pseudo*-C_{2v} solid-state structure. Two distinct resonances central arene protons are observed at 5.65 and 4.57 ppm, consistent with strong metal-arene backbonding. Two methine signals (2.30, 2.11 ppm) and a single resonance (50.32 ppm) are observed by ^{1}H and ^{31}P{^{1}H} NMR, respectively. The terminal carbon monoxide ligand of complex **13-CO** is readily substituted upon addition of trimethylphosphine (PMe_3) to yield complex **13-PMe₃** (Scheme 3). While single crystals suitable for XRD analysis have not been obtained to date due to the compound's high solubility, spectroscopic characterization of the complex indicates an intact triangulo-trinickel core. The C_s symmetry of complex **13-CO** has not been perturbed by PMe_3 substitution as two ^{1}H NMR resonances corresponding to the methine protons are observed (2.41 and 2.24 ppm). The ^{31}P{^{1}H} NMR spectrum of **13-PMe$_3$** displays the terphenyl phosphines as a doublet at 51.49 ppm and the PMe_3 as a triplet at -6.61 ppm; the observed multiplicity is consistent with the assigned structure. Strong metal-arene interactions are also maintained based on the upfield-shifted ^{1}H NMR resonances at 5.12 and 4.67 ppm. The substitution of the terminal CO ligand is supported by the IR spectrum, showing only bands indicative of bridging CO ligands (1854, 1783 cm^{-1}) and the disappearance of the peak at 195.08 ppm (^{13}C NMR) observed for complex **13-CO**. The increased electron density of Ni3 induced by the ligand substitution is reflected in the 0.53 upfield shift of the arene C-*H* ^{1}H NMR peak compared to **13-CO** and the lower stretching energy of the bridging CO ligands. The lability of this terminal CO ligand suggests that coordination and activation of other molecules at the Ni_3 unit in **13-CO** may be possible.

The IR spectrum of complex **9** displays peaks corresponding to terminal CO stretches at 1966, 1914, 1903, and 1880 cm^{-1}. This is comparable to an asymmetrically substituted [FeFe]-hydrogenase model complex, (μ-pdt)[$Fe^I(CO)_2(PMe_3)$][$Fe^I(CO)_2$(IMes)] (pdt = 1,3-propanedithiolate, IMes = 1,3-bis(2,4,6-trimethylphenyl)imidazol-2-ylidene), with CO stretches at 1972, 1933, 1897, and 1882 cm^{-1}.[20] Complex **11** shows peaks consistent with the presence of two terminal (1946 and 1928 cm^{-1}) and one bridging (1771 cm^{-1}) CO ligands, as observed in the solid-state.[21] Similarly, complex **12** shows IR absorptions for two terminal (1972, 1952 cm^{-1}) and one bridging (1803 cm^{-1}) CO ligands.[21]

Cyclic voltammetry (CV) studies of complex **9** revealed a quasireversible oxidation at -0.44 V versus the Fc/Fc$^+$ couple (Figure 15). Complexes **11** and **12** did not show reversible redox events in CV studies, and chemical oxidations led to decomposition. The addition of one equivalent of ferrocenium hexafluorophosphate to a THF solution of complex **9** resulted in a color change from orange-red to green. The one-electron oxidized complex, **10**, was isolated in 41% yield, but was found to be unstable in solution at ambient temperatures. However, crystals of complex **10** grown at -35 °C were stable for weeks in the solid-state and proved suitable for XRD analysis.

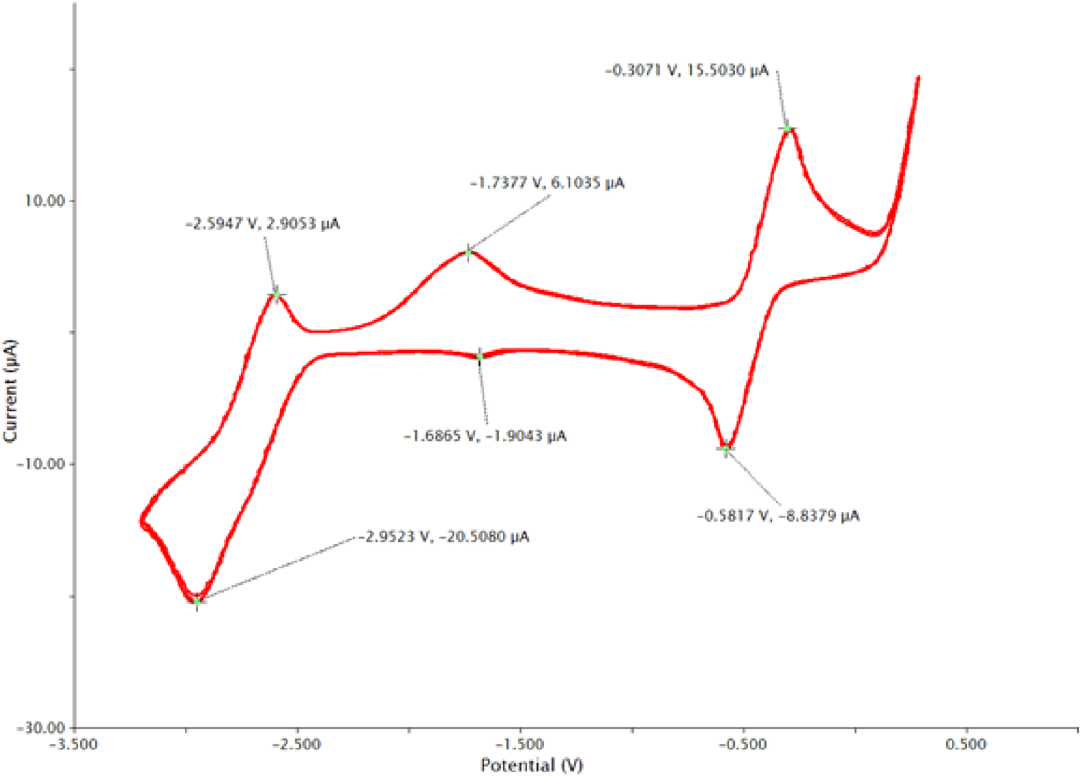

Figure 15. Cyclic voltammogram of **9** with potentials referenced to the Fc/Fc^+ couple.

Oxidation of complex **9** results in significant structural changes to both the coordination mode of the Fe_2 core to the central arene and the nature of the central arene deplanarization (Figure 11). The diiron core binds in an μ_2:(η^2,η^4) fashion, consistent with a distorted neutral ene-diene assignment for the arene. The longest C–C distances are C1–C2 and C3–C4 (average of 1.467 Å), which correspond to the bonds separating the metal-bound olefin and diene fragments. This is an unusual structural motif for an arene coordinated to a dinuclear unit. The Fe–Fe bond of **10** has contracted to 2.6320(3) Å, over 0.12 Å shorter compared to complex **9**. This is suggestive of a strengthened metal–metal bonding interaction and is in agreement with the shorter Fe–Fe bond of 2.423 Å observed in a comparatively more oxidized literature μ_2-arene Fe_2 complex.[15c] The IR spectrum of **10** shows peaks at 2010, 1972, 1938, and 1917 cm^{-1} consistent with terminal CO stretches. These values are indicative of weaker back-bonding from metal to CO in **10** compared to **9**, consistent with a higher formal oxidation state in the former. The aforementioned [FeFe]-hydrogenase model complex has been chemically oxidized by one electron and also shows higher terminal CO stretching frequencies at 2036, 1997, and 1987 cm^{-1},[20] with shifting of the IMes ligand from an apical to a basal position. Given the trans-spanning nature of the phosphine arms in compound **1**, such a rearrangement is not readily accommodated and instead M–arene coordination is perturbed from μ_2:(η^3,η^3) to give a *pseudo*-square pyramidal geometry around Fe1. The neutral ene-diene assignment of the central arene challenges a formal oxidation state assignment of **10** as $Fe^{I}Fe^{II}$ and underscores the potential redox participation of the central arene in the interconversion of **9** and **10**. Such ambiguity in formal oxidation state assignments is not uncommon for non-innocent ligands.[22] Although the central arene may also be regarded as a formal electron acceptor and redox non-innocent ligand, its most notable aspect is the ability to accommodate a variety of coordination modes and support reversible electron-transfer chemistry at the Fe_2-(μ_2-arene) unit.

CONCLUSIONS

In summary, the synthesis of new series of hetero- and homometallic multinuclear clusters was accomplished. In Section 2.2, access to a family of structurally related heterometallic trinuclear complexes allowed for the systematic study of the effects of changes in metal composition and ligand electronics. The identity of the minor, apical metal significantly impacts the C–O stretching frequency, as expected given the weak M–M' interaction and changes in Pd–arene interactions. The identity of the homodinuclear moiety metal of the bimetallic core also affects the CO stretching frequency, $^{31}P\{^{1}H\}$ NMR chemical shifts, and Mössbauer parameters. Ligand electronics were found to affect the spectroscopic features of the clusters, but to a lesser extent than changes in metal identity. Electrochemical behavior varied considerably with metallic composition and nature of the supporting arene. Overall, the present studies provide a quantitative evaluation of the effect of metal identity and supporting ligands in triangular low oxidation state metal clusters. Future studies with these complexes focuses on gaining further insight into heterometallic effects on chemical and physical properties of transition metal clusters.

The discussed homometallic multinuclear Fe, Co, and Ni complexes presented in Section 2.3 show that the combination of pendant donors surrounding an arene moiety provides a versatile multidentate platform to support a variety of multinuclear complexes of first-row transition metals. Beyond the intriguing structural aspects, the redox-induced reorganization of the arene highlights its flexible coordination modes and the ability to accommodate electron transfer chemistry. Future work will focus on employing the redox non-innocence and coordination lability of π-bound aromatic systems for reactivity.

EXPERIMENTAL SECTION

General considerations.

All air- and/or water-sensitive compounds were manipulated using standard vacuum or Schlenk line techniques or in an inert atmosphere glove box. The solvents for air- and moisture-sensitive reactions were dried over sodium benzophenone ketyl, calcium hydride, or by the method of Grubbs.[23] All NMR solvents were purchased from Cambridge Isotopes Laboratories, Inc. and dried over sodium benzophenone ketyl or calcium hydride. Unless mentioned otherwise, reagents were used as received from commercial suppliers without further purification. Bis(1,5-cyclooctadiene)nickel(0), nickel(II) dichloride dimethoxyethane adduct, $Fe_3(CO)_{12}$ stabilized with 10 wt. percent methanol, tetrakis(acetonitrile)palladium(II) tetrafluroborate, cobaltocene, and tris-(dibenzylideneacetone)dipalladium(0) were ordered from Strem Chemicals, Inc. 2-bromophenylboronic acid was purchased from Ark Pharm, Inc. Chlorodiisopropylphosphine, ferrocenium hexafluorophosphate, and carbon monoxide were purchased from Sigma Aldrich. Iodine monochloride, $Co_2(CO)_8$, [*n*Bu_4N][PF_6], and ferrocene were purchased from Alfa Aesar. 1,4-dimethoxy-2,5-diiodobenzene,[24] 1,4-bis(2-diisopropylphosphinophenyl)benzene,[8] compounds **1** and **7**,[8] $[Pd(MeCN)_3]_2[BF_4]_2$,[25] $Na[Co(CO)_4]$,[26] and $Na_2[Fe(CO)_4]$[27] were synthesized according to literature procedures. All ^1H, ^{13}C, and ^{31}P spectra were recorded on Varian Mercury 300 MHz, or Varian INOVA-500 or 600 MHz spectrometers at room temperature. Chemical shifts for ^1H and ^{13}C NMR data are reported relative to residual solvent peaks and are ^{13}C and ^1H decoupled, respectively, unless otherwise noted.[28] ^{31}P NMR chemical shifts are reported with respect to the deuterated solvent used to lock the instrument and are ^1H decoupled unless otherwise noted. IR spectra were obtained as solution samples using a CaF_2 window cell on a Thermo Scientific Nicolet

6700 FT-IR spectrometer or as thin films on a Bruker Alpha FT-IR spectrometer with a diamond ATR attachment. Elemental analyses were performed by Robertson Microlit Laboratories, Ledgewood, NJ.

Synthesis of 1,4-bis(2-bromophenyl)-2,5-(dimethoxy)benzene (B-R) (R = -OMe)

The Suzuki coupling to produce the terphenyl product was run as a modification of literature procedure.[8] A Schlenk tube fitted with a Teflon stopper was charged with 1,4-dimethoxy-2,5-diiodobenzene (5.00 g, 12.82 mmol, 1 equiv.), 2-bromo-phenylboronic acid (5.41 g, 26.9 mmol, 2.1 equiv.), and K_2CO_3 (10.63 g, 76.9 mmol, 6 equiv.). Toluene (270 mL), ethanol (65 mL), and water (65 mL) were then transferred to the Schlenk tube along with a magnetic stirbar. The mixture was degassed by two freeze pump thaw cycles and then put under positive nitrogen pressure. Under a strong counterflow of nitrogen, $Pd(PPh_3)_4$ (741 mg, 0.64 mmol, 0.05 equiv.) was added and the solution became a pale yellow color. The reaction mixture was then heated to 65 ºC and stirred for 16-24 hrs while monitoring the reaction by GC-MS. The volatiles were then removed on a rotovap and the residue triturated with water, then methanol, and finally dichloromethane to yield the product as an off-white powder. Yield: 4.22 g (67 %). ^{1}H NMR (500 MHz, $CDCl_3$) δ 7.42-7.36 (unresolved m, 4H, aryl-*H*), 7.23 (m, 2H, aryl-*H*), 6.82 (s, 2H, central aryl-*H*), 3.74 (s, 6H, OC*H*$_3$). ^{13}C NMR (126 MHz, $CDCl_3$) δ 150.20 (s), 129.61 (s), 132.64 (s), 131.68 (s), 130.35 (s), 128.82 (s), 127.04 (s), 124.13 (s), 114.45 (s), 56.39 (s). GC-MS (m/z): Calcd, 447.95 (M^+), Found: 448.1 (M^+). FAB-MS (m/z): Calcd, 447.9496 (M^+), Found: 447.9486 (M^+).

Synthesis of 1,4-bis(2-(diisopropylphophino)phenyl)-2,5-(dimethoxy)benzene (1-(OMe)$_2$)

Phosphination run as a modification of literature procedures.[8] A Schlenk tube fitted with a screw-in Telfon stopper was charged with 1,4-bis(2-bromophenyl)-2,5-dimethoxybenzene (1.5 g, 3.34 mmol, 1 equiv.) and a magnetic stirbar. Tetrahydrofuran (150 mL) was then to the Schlenk tube. The reaction was cooled to -78 ºC and *tert*-butyllithium (1.7 M pentane solution, 8 mL, 13.7 mmol, 4.1 equiv.) was added while stirring to generate a pale yellow solution. The reaction mixture was allowed to warm to room temperature and then stirred for an additional hour. During this time the solution became a cloudy suspension. Chlorodiisopropyl phosphine (1.12 mL, 7.02 mmol, 2.1 equiv.) was then added to the reaction via syringe. The solution immediately became a homogenous pale yellow solution which was allowed to stir for 16 hours. The volatiles were then removed under reduced pressure on the Schlenk line. The yellowish residue was then suspended in *ca.* 100 mL of toluene and filtered through a Celite pad. The filtrate was then dried under reduced pressure. This residue was then triturated with acetonitrile (*ca.* 20 mL) which removed colored impurities to leave the product as a white powder. Yield: 0.6 g (34 %). ^{1}H NMR spectra of product is broad at room temperature due to hindered rotation around aryl–aryl bonds. This is corroborated by ^{31}P NMR, where two distinct peaks are observed at room temperature. ^{1}H NMR (300 MHz, C_6D_6) δ 7.49 (m, 2H, aryl-*H*), 7.43 (m, 2H, aryl-*H*), 7.19 (m, 4H, aryl-*H*), 6.83 (s, 2H, central aryl-*H*), 3.43 (s, 6H, OC*H*$_3$), 2.05 (m, 2H, C*H*), 1.87 (m, 2H, C*H*), 1.06 (m, 24H, C*H*$_3$). ^{31}P{^{1}H} NMR (121 MHz, C_6D_6) δ -1.18 (s), -2.67 (s). This is due to the formation of two different atropisomers at room temperature due to hindered rotation around the aryl-aryl bonds. A single ^{31}P resonance is observed at -0.2 ppm at 70 ºC. ^{13}C{^{1}H} NMR (126 MHz, C_6D_6) δ 149.98

(s), 147.34 (d, J_{PC} = 30.5 Hz), 136.26 (d, J_{PC} = 22.0 Hz), 131.97 (s), 130.90 (s), 130.65 (s), 128.12 (s), 126.33 (s), 115.02 (s), 54.93 (s), 25.42 (broad s), 24.03 (broad s), 23.38 (broad s), 20.35 (broad s), 19.89 (broad s), 19.12 (broad s). GC-MS (m/z): Calcd: 522.28 (M^+), Found: 521.2761. FAB-MS (m/z): Calcd: 521.2738 (M^+), Found: 521.2761 (M^+).

Synthesis of Complex 3

Compound **2** was generated *in situ* from the reaction of 1,4-bis(2-diisopropylphosphinophenyl)benzene (**1**) (100 mg, 0.216 mmol, 1 equiv.) with $[Pd(MeCN)_3]_2[BF_4]_2$ (MeCN = acetonitrile) (136.8 mg, 0.216 mmol, 1 equiv.). This was accomplished by charging a 20 mL scintillation vial with the 1,4-bis(2-diisopropylphosphinophenyl)benzene and a magnetic stirbar before adding the $[Pd(MeCN)_3]_2[BF_4]_2$ as a solution in acetonitrile (*ca.* 5 mL) and allowing the mixture to stir over 1 hr at room temperature. During this time the solution became a homogeneous red. Formation of **1** could be confirmed by ^{31}P NMR of reaction mixture. $Na_2[Fe(CO)_4]$ was added as a partially solubilized suspension in tetrahydrofuran (*ca.* 2 mL) at room temperature. The solution immediately became a darker red and the reaction was allowed to stir for 1 hr. Volatiles were then removed under reduced pressure. The residue was suspended in acetonitrile and filtered onto a Celite pad. The solid was washed with additional acetonitrile until washes became colorless. The remaining material was dissolved in tetrahydrofuran filtered through the Celite pad. Removal of volatiles yielded the product as a red solid. Yield: 80 mg (44 %). Single crystals suitable for X-ray diffraction studies were grown from the vapor diffusion of hexanes into a concentrated tetrahydrofuran:benzene (1:1) solution at room temperature. ^{1}H NMR (300 MHz, C_6D_6) δ 7.18 (s, 2H, aryl-*H*), δ 7.11-6.98 (m, 6H, aryl-*H*), δ 5.92 (s, 4H, central aryl-*H*), δ 2.26 (m, 4H, C*H*), δ 1.25 (dd, J_{PH} = 18.1, J_{HH} = 7.0 Hz, 12H, CH_3), δ 0.89 (dd, J_{PH} = 8.5, J_{HH} = 7.2 Hz, 12H, CH_3). ^{31}P{^{1}H} NMR (121 MHz, C_6D_6) δ 53.36 (s). ^{13}C{^{1}H} NMR (126 MHz, CD_2Cl_2) δ 225.26 (s), 149.04 (vt, J_{PC} = 14.0 Hz), 141.36 (vt, J_{PC} = 14.3 Hz), 132.80 (s), 132.17 (vt, J_{PC} = 7.0 Hz), 130.66 (s), 128.19 (s), 118.03 (s), 111.15 (s), 26.62 (vt, J_{PC} = 8.4 Hz), 19.33 (s), 18.64 (s). IR (CaF_2 window, C_6H_6, cm^{-1}) ν_{CO}: 1901 (s), 1874 (m), 1848 (s), 1843 (w, sh). Anal. Calcd. for: $C_{34}H_{40}FeO_4P_2Pd_2$ (**3**) (%): C, 48.42; H, 4.78. Found: C, 48.25; H, 5.08.

Synthesis of Complex 4

Compound **3** was generated in an analogous fashion to the procedure described in the synthesis of **3** again using 4-bis(2-diisopropylphosphinophenyl)benzene (40 mg, 0.0865 mmol, 1 equiv.) and $[Pd(MeCN)_3]_2[BF_4]_2$ (MeCN = acetonitrile) (54.7 mg, 0.0865 mmol, 1 equiv.). To the *in situ* generated acetonitrile solution of **2** was added [Na][Co(CO)$_4$] (16.8 mg, 0.0865 mmol, 1 equiv.) as an acetonitrile solution (*ca.* 2 mL). The reaction mixture was allowed to stir for 1 hr at room temperature. During this time the reaction mixture turned a deep purple-red. The volatiles were then removed under reduced pressure. The residue was then suspended in benzene and collected on a Celite pad. The solid was then washed with additional benzene until the washes became colorless. The washed solid was then dissolved in tetrahydrofuran and filtered through the Celite pad. Removal of volatiles yielded the product as a purple-red solid. Yield: 40 mg, (49 %). Single crystals suitable for X-ray diffraction were grown by the vapor diffusion of hexanes into a concentrated tetrahydrofuran:benzene solution at room temperature. ^{1}H NMR (300 MHz, CD_3CN) δ 7.92-7.62 (m, 8H, aryl-*H*), 6.39 s, 4H, central aryl-*H*), 2.72 (m, 4H, C*H*), 1.18 (m, 24H, C*H*$_3$). ^{31}P{^{1}H} NMR (121 MHz, CD_3CN) δ 61.83 (s). ^{19}F NMR (282 MHz, CD_3CN) δ 61.83 (s).^{13}C{^{1}H} NMR (126 MHz, CD_3CN) δ 203.70 (broad), 146.58 (vt, J_{PC} = 12.6 Hz), 136.83 (vt, J_{PC} = 17.7 Hz), 133.50 (s), 132.60 (s), 132.23 (s), 129.77 (s), 116.42 (s), 114.30 (s), 26.40 (s), 18.84 (s), 18.04 (s). IR (CaF_2 window, THF, cm^{-1}) ν_{CO}: 2057 (s), 2012 (m), 1915 (m), 1878 (w, sh). Anal. Calcd. for: $C_{34}H_{40}BCoF_4O_4P_2Pd_2$ (**4**) (%): C, 43.76; H, 4.32. Found: C, 43.58; H, 4.48.

Synthesis of Complex 5

Compound **4** (50 mg, 0.0535 mmol, 1 equiv.) was added to a 20 mL scintillation vial. Tetrahydrofuran (*ca*. 5 mL) was added to fully dissolve **4**. Cobaltocene (10.1 mg, 0.0535 mmol, 1 equiv.) was added as a tetrahydrofuran solution (1 mL) and the reaction mixture was allowed to stir for 1 hr. During this time the solution changed from purple-red to a green-brown. The volatiles were removed under reduced pressure. The residue was suspended in hexanes and collected over a Celite pad. The solid was washed with hexanes until only a pale green tinge remained in the washes which were initially brown. The remaining green colored material was dissolved in benzene and brought through the Celite pad. The benzene filtrate was then dried to a solid under reduced pressure. The benzene soluble material was then dissolved in minimal diethyl ether and then several drops of hexamethyldisiloxane were added. The product was then precipitated by the slow evaporation of diethyl ether. Yield: 14 mg (31 %). The product is unstable and prone to decomposition. Therefore characterization was obtained immediately after synthesis. Single crystals were obtained from the vapor diffusion of diethyl ether out of a concentrated solution of **5**. IR (CaF_2 window, THF, cm^{-1}) ν_{CO}: 2007 (s), 1920 (m, sh), 1879 (m), 1837 (m). Anal. Calcd. for: $C_{34}H_{40}CoO_4P_2Pd_2$ (**5**) (%): C, 48.25; H, 4.76. Found: C, 48.24; H, 4.61.

Synthesis of Complex 3-(OMe)$_2$

A Schlenk tube fitted with a screw-in Telfon stopper was charged with **1-(OMe)$_2$** (100 mg, 0.191 mmol, 1 equiv.) and a magnetic stirbar. $[Pd(MeCN)_3]_2[BF_4]_2$ (MeCN = acetonitrile) (121 mg, 0.191 mmol, 1 equiv.) was transferred as an acetonitrile solution (*ca.* 20 mL) and the mixture was allowed to stir at room temperature for 1 hr. During this the time the reaction mixture became a homogenous deep red. $[Na]_2[Fe(CO)_4]$ (40.9 mg, 0.191, 1 equiv.) was then added as a partially solubilized tetrahydrofuran suspension (*ca.* 2 mL) and the reaction was allowed to stir for 1 hr at room temperature. The volatiles were then removed under reduced pressure. The residue was triturated with hexanes and collected over a Celite pad. The solid was then washed with additional hexanes until the washes became colorless. Then 10 mL of cold ether were used to wash the solid. The remaining solid was dissolved in benzene and brought through the Celite pad. Removal of volatiles yielded the product as a red solid. Yield: 40 mg (23 %). Crystals suitable for X-ray diffraction studies were grown from the vapor diffusion of hexanes into a concentrated tetrahydrofuran:benzene (1:1) solution. ^1H NMR (300 MHz, C_6D_6) δ 7.47 (d, J_{HH} = 7.6 Hz, 2H, aryl-*H*), 7.28 (m, 2H, aryl-*H*), 7.20 (m, 2H, aryl-*H*), 7.09 (t, J_{HH} = 7.4 Hz, 2H, aryl-*H*), 5.55 (s, 2H, central aryl-*H*), 2.94 (s, 6H, OCH_3), 2.40 (m, 2H, C*H*), 2.27 (m, 2H, C*H*), 1.33 (m, 12H, CH_3), 0.99 (aq, J_{HH} = 7.2 Hz, 6H, CH_3), 0.91 (aq, J_{HH} = 7.2 Hz, 6H, CH_3). $^{31}P\{^1H\}$ NMR (121 MHz, C_6D_6) δ 56.92 (s). $^{13}C\{^1H\}$ NMR (126

MHz, CD_2Cl_2) δ 225.48 (s), 147.08 (vt, J_{PC} = 14.7 Hz), 143.24 (vt, J_{PC} = 15.0 Hz), 140.86 (s), 132.70 (s), 132.20 (vt, J_{PC} = 7.6 Hz), 130.83 (s), 128.05 (s), 54.90 (s), 26.84 (d, J_{PC} = 8.6 Hz), 26.71 (d, J_{PC} = 8.4 Hz), 19.56 (vt, J_{PC} = 5.1 Hz), 19.41 (vt, J_{PC} = 4.6 Hz), 18.77 (s), 18.53 (s). IR (CaF_2 window, C_6H_6, cm^{-1}) ν_{CO}: 1898, 1867, 1838 (fourth IR stretch likely coincidentally underneath 1838 band by analogy to the IR of compound **3**). Anal. Calcd. for: $C_{36}H_{44}FeO_6P_2Pd_2$ (**3-(OMe)$_2$**) (%): C, 47.86; H, 4.91. Found: C, 48.14 H, 4.86.

Synthesis of Complex 8

A Schlenk tube fitted with a screw-in Teflon stopper was charged with **7** (300 mg, 0.462 mmol, 1 equiv.) and a magnetic stirbar. Tetrahydrofuran (*ca.* 20 mL) was then transferred to the Schlenk tube to yield a green homogeneous solution. $[Na]_2[Fe(CO)_4]$ (100.7 mg, 0.462 mmol, 1 equiv.) was added as a partially solubilized tetrahydrofuran suspension (*ca.* 10 mL). This addition resulted in an immediate color change from green to brown within a minute. The reaction mixture was allowed to stir at room temperature for 1 hr. Volatiles were then removed under reduced pressure. The dark brown residue was suspended in hexanes and filtered on a Celite pad. The solid was then washed with hexanes until the washes were colorless. The remaining solid was then washed with 10 mL cold diethyl ether. Finally, the product was dissolved with benzene and brought through the Celite pad. The benzene soluble material was lyophilized to yield the product as a brown powder. Yield: 160 mg (41 %). Crystals suitable for X-ray diffraction studies could be grown from the slow vapor diffusion of hexanes into a concentrated tetrahydrofuran:benzene (1:1) solution. However, the compound decomposes in solution over extended periods of time and the cleanest material was obtained without crystallization. ^{1}H NMR (300 MHz, C_6D_6) δ 7.17 (d, J_{HH} = 7.4 Hz, 2H, aryl-*H*), 7.05-6.90 (m, 6H, aryl-*H*), 5.78 (s, 4H, central aryl-*H*), 2.32 (h, J_{HH} = 7.0 Hz, 4H, C*H*), 1.19 (m, 12H, CH_3), 0.89 (aq, J_{HH} = 7.0 Hz, CH_3). ^{31}P{^{1}H} NMR (121 MHz, C_6D_6) δ 43.18 (s). ^{13}C{^{1}H} NMR (126 MHz, C_6D_6) δ 225.38 (broad s), 150.24 (vt, J_{PC} = 14.2 Hz), 138.27 (vt, J_{PC} = 15.0 Hz), 131.40 (s), 130.23 (s), 130.09 (s), 127.70 (s), 103.31 (s), 102.02 (s), 25.18 (vt, J_{PC} = 9.7 Hz), 18.60 (s), 17.66 (s). IR (CaF_2 window, C_6H_6, cm^{-1}) ν_{CO}: 1896, 1874, 1821, 1798.3 (sh). Anal. Calcd. for: $C_{34}H_{40}FeO_4P_2Ni_2$ (**8**) (%): C, 54.60; H, 5.39. Found: C, 54.69; H, 5.35.

Synthesis of Complex 6

Compound **2** (82.7 mg, 0.089 mmol, 1 equiv.) was transferred to a 20 mL scintillation vial equipped with a magnetic stirbar. Acetonitrile (*ca.* 5 mL) was then added to dissolve the compound and then $Mo(CO)_3(MeCN)_3$ (27.2 mg, 0.089 mmol, 1 equiv.) was then added as a suspension in *ca.* 1 mL acetonitrile. Following addition of the molybdenum precursor the reaction mixture immediately became homogeneous. After 1 hr, volatiles were removed under reduced pressure and the solid residue was triturated with THF until washes became colorless leaving behind clean material as a red solid. Yield: 77 mg (75.2 %). ^{1}H NMR (300 MHz, CD_3CN) δ 7.86 – 7.80 (m, 2H, Ar*H*), 7.79 – 7.68 (m, 4H, Ar*H*), 7.55 (dd, *J* = 7.7, 1.5 Hz, 2H, Ar*H*), 6.50 (s, 4H, central-Ar*H*), 2.83 – 2.67 (m, 4H, C*H*), 1.26 – 1.10 (m, 24H, CH_3). ^{13}C NMR (126 MHz, CD_3CN δ 230.16 (s), 146.16 (vt, J_{CP} = 12.1 Hz), 135.07 (vt, J_{CP} = 18.5 Hz), 133.35 (s), 132.61 (s), 132.13 (vt, J_{CP} = 7.1 Hz), 129.91 (s), 126.56 (s), 123.43 (s), 25.69 (t, J_{CP} = 9.9 Hz), 18.06 (s), 17.41 (s). ^{31}P NMR (121 MHz, CD_3CN) δ 56.87. ^{19}F NMR (282 MHz, CD_3CN) δ -151.77.

Synthesis of Complex 4-(OMe)$_2$

1-(OMe)$_2$ (55.1 mg, 0.105 mmol, 1 equiv.) was transferred to a 20 mL scintillation vial equipped with a magnetic stirbar. [Pd(MeCN)$_3$]$_2$[BF$_4$]$_2$ (MeCN = acetonitrile) (66.7 mg, 0.105 mmol, 1 equiv.) was transferred as an acetonitrile solution (*ca.* 5 mL) and the mixture was allowed to stir at room temperature for 1 hr. During this the time the reaction mixture became a homogenous deep red. [Na][Co(CO)$_4$] (20.88 mg, 0.105 mmol, 1 equiv.) was then added as a solution in *ca.* 5 mL acetonitrile and the reaction mixture was allowed to stir for 1 hr at room temperature. During this time the reaction mixture turned a deep purple-red. The volatiles were then removed under reduced pressure. The residue was then suspended in benzene and collected on a Celite pad. The solid was then washed with additional benzene until the washes became colorless. The washed solid was then dissolved in tetrahydrofuran and filtered through the Celite pad. Removal of volatiles yielded the product as a purple-red solid. ^{1}H NMR (300 MHz, CD$_3$CN) δ 7.90 – 7.62 (m, 1H), 5.80 (s, 0H), 3.25 (s, 1H), 2.83 – 2.61 (m, 1H), 1.36 – 1.25 (m, 1H), 1.20 – 1.07 (m, 3H). ^{31}P NMR (121 MHz, CD$_3$CN) δ 64.99. ^{19}F NMR (282 MHz, CD$_3$CN) δ -151.87.

Synthesis of Complex 7-(OMe)$_2$

Compound **1-(OMe)$_2$** (300 mg, 0.574 mmol, 1 equiv.) was transferred to a 20 mL scintillation vial equipped with a magnetic stirbar. Ni(COD)$_2$ (158.3 mg, 0.574 mmol, 1 equiv.) was then added as a suspension in THF (*ca.* 5 mL). The reaction mixture was allowed to stir for 10 min during which time the solution turned a deep red. NiCl$_2$dme (126 mg, 0.574 mmol, 1 equiv.) was then added as a suspension in minimal THF, resulting in formation of a green solution. The reaction mixture was allowed to stir for 24 hrs before volatiles were removed under reduced pressure to yield a green powder which was carried on to the synthesis of **8-(OMe)₂** without further purification. ^{1}H NMR (300 MHz, Benzene-d_6) δ 7.43 (d, *J* = 7.8 Hz, 1H), 7.03 (t, *J* = 7.1 Hz, 1H), 6.90 (t, *J* = 7.3 Hz, 1H), 6.82 (d, *J* = 7.4 Hz, 1H), 6.30 (s, 1H), 3.78 (s, 3H), 1.86 (t, *J* = 6.9 Hz, 0H), 1.77 (q, *J* = 7.0 Hz, 1H), 1.37 (d, *J* = 6.9 Hz, 4H), 1.26 (d, *J* = 7.0 Hz, 4H), 1.01 (d, *J* = 6.9 Hz, 4H), 0.93 (d, *J* = 6.8 Hz, 4H). ^{31}P NMR (121 MHz, Benzene-d_6) δ 64.74.

Synthesis of Complex 8-(OMe)$_2$

Compound **7-(OMe)$_2$** (40 mg, 0.0563 mmol, 1 equiv.) was transferred to a 20 mL scintillation vial equipped with a magnetic stirbar as a solution in THF (*ca.* 4 mL). To the rapidly stirring solution was added $[Na]_2[Fe(CO)_4]$ (12.1 mg, 0.0563 mmol, 1 equiv.) as a suspension in *ca.* 1 mL THF. The reaction mixture was allowed to stir for 1 hr before volatiles were removed under reduced pressure to yield a brown residue. The residue was triturated with hexanes and filtered over a Celite pad until washes became colorless. The solid was then washed with a small portion of diethyl ether. The remaining material was dissolved in benzene and brought through the Celite pad and lyophilized to afford the product as a brown solid. ^{1}H NMR (300 MHz, C_6D_6) δ 7.41 (d, *J* = 7.7 Hz, 2H, Ar*H*), 7.15 – 7.05 (m, 4H, Ar*H*), 6.98 (t, *J* = 7.3 Hz, 2H, Ar*H*), 5.30 (s, 2H, central-Ar*H*), 3.27 (s, 6H, OC*H*$_3$), 2.73 – 2.57 (m, 2H, C*H*), 2.11 (m, 2H, C*H*), 1.49 – 1.39 (m, 6H, C*H*$_3$), 1.20 – 1.10 (m, 6H, C*H*$_3$), 0.98 – 0.90 (m, 12H, C*H*$_3$). ^{31}P NMR (121 MHz, C_6D_6) δ 44.99.

Synthesis of Complex 9

Compound **1** (300 mg, 0.648 mmol, 1 equiv) was transferred as a solution in *ca.* 10 mL THF into a quartz Schlenk tube fitted with a screw-in Teflon stopper along with a magnetic stir bar. $Fe_3(CO)_{12}$ (10 wt % MeOH stabilizer) (359.3 mg, 0.648 mmol, 1 equiv) was then added as a solution in *ca.* 20 mL THF. The reaction mixture was then thoroughly degassed and allowed to stir for 1 hr, during which time the solution turned from green to a deep red. The reaction mixture was then subjected to UV photolysis under a 200 W Hg-Xe lamp for 2-3 days until the desired product was determined to be the majority species by ^{31}P NMR. During photolysis, the solution was degassed every few hours. Volatiles were then removed under reduced pressure. The dark red/orange residue was washed with hexanes then diethyl ether until only a pale orange color remained in washes. The remaining material was dissolved in THF and filtered through a Celite pad and the filtrate dried under reduced pressure. The solid was then recrystallized by the vapor diffusion of hexanes into a concentrated THF solution. Resulting dark red/orange crystals were washed with hexanes and dried under reduced pressure. Yield: 48.4 mg (11 %) ^1H NMR (300 MHz, C_6D_6) δ 7.57 (d, 2H, aryl-*H*), 7.10 (t, 2H, aryl-*H*), 6.97 (t, 2H, aryl-*H*), 6.88 (t, 2H, aryl-*H*), 3.76 (s, 4H, central aryl-*H*), 2.20 (m, 4H, C*H*), 0.98 (dd, 12H, CH_3), 0.82 (dd, 12H, CH_3) ppm. ^{31}P NMR (121 MHz, C_6D_6) δ 90.59 (s) ppm. ^{13}C NMR (126 MHz, C_6D_6) δ 221.3 (d), 149.4 (d), 139.0 (d), 130.2 (d), 129.3 (s), 129.0 (s), 126.84 (s), 96.8 (s), 57.6 (s), 26.7 (d), 17.2 (d) ppm. IR (ATR film, cm^{-1}) ν_{CO}: 1966, 1914, 1903, 1880. Anal. Calcd. for: $C_{34}H_{40}Fe_2O_4P_2$ (**9**) (%): C, 59.50; H, 5.87. Found: C, 59.29; H, 5.74.

Synthesis of Complex 11

Compound **1** (100 mg, 0.216 mmol, 1 equiv) was transferred as a solution in *ca.* 15 mL toluene into a Schlenk tube fitted with a screw-in Teflon stopper along with a magnetic stir bar. $Co_2(CO)_8$ (74 mg, 0.216 mmol, 1 equiv) was then added as a solution in *ca.* 15 mL toluene. The brown reaction mixture was heated to 110 ºC for 1 hour. The solution was then degassed, 1 atm of fresh N_2 readmitted, and then heated at 110 ºC for an additional 2-3 hours. During this time the solution turned green. The reaction mixture was then dried under reduced pressure. The green powder was washed with *ca.* 10 mL of ether and the remaining material dissolved in THF and filtered through a Celite pad and dried under reduced pressure to yield a green powder as the clean product. Yield: 78 mg (54 %). ^{1}H NMR (300 MHz, C_6D_6) δ 7.51 (d, 2H, aryl-*H*), 7.14 (t, 2H, aryl-*H*), 7.05 (t, 2H, aryl-*H*), 6.93 (m, 2H, aryl-*H*), 4.29 (broad s, 2H, central aryl-*H*), 3.95 (d, 2H, central aryl-*H*), 2.90 (m, 2H, C*H*), 2.19 (m, 2H, C*H*), 1.15 (m, 12H, CH_3), 0.99 (dd, 6H, CH_3), 0.89 (dd, 6H, CH_3) ppm. ^{31}P NMR (121 MHz, C_6D_6) δ 80.20 (s) ppm. ^{13}C NMR (126 MHz, C_6D_6) δ 271.45 (s), 215.4 (s), 153.21 (d), 135.25 (d), 130.40 (s), 129.46 (s), 127.65 (s), 127.42 (m), 87.39 (s), 61.65 (d), 60.15 (s), 27.29 (t), 24.51 (s), 18.32 (s), 18.13 (s), 17.86 (s), 17.28 (s) ppm. IR (CaF_2 window, THF, cm^{-1}) ν_{CO}: 1946, 1928, 1771. Anal. Calcd. for: $C_{33}H_{40}Co_2O_3P_2$ (**11**) (%): C, 59.65; H, 6.07. Found: C, 59.90; H, 6.07.

Synthesis of Complex 12

Complex **7** (100.0 mg, 0.154 mmol, 1 equiv) was transferred as a solution in *ca.* 6 mL of THF into a 20 mL scintillation vial along with a magnetic stir bar. [Na][Co(CO)$_4$] (29.8 mg, 0.154 mmol, 1 equiv) was then added as a solution in *ca.* 4 mL of THF. The reaction mixture was stirred for 30 minutes at room temperature, during which time the solution turned from green to brown/yellow. The solution was then dried under reduced pressure, and the resulting solid was triturated with diethyl ether, filtered through a Celite pad, and then dried under reduced pressure. The solid from the filtrate was recrystallized by the vapor diffusion of pentane into a concentrated THF solution to yield ruby red rectangular crystals. Complex **12** is *unstable* in solution and slowly decomposes to two different products by ^{31}P NMR at 50.32 (**13-CO**) and 32.31 ppm.[7a] Yield: 11 mg (11 %) ^{1}H NMR (300 MHz, C_6D_6) δ 7.26 (broad d, 2H, aryl-*H*), 7.15-6.96 (broad m, 6H, aryl-*H*), 5.85 (broad s, 4H, central aryl-*H*), 2.32 (m, 4H, C*H*), 1.44-0.80 (broad m, 24H, C*H₃*) ppm. ^{31}P NMR (121 MHz, C_6D_6) δ 34.80 (s) ppm. ^{13}C NMR (126 MHz, C_6D_6) δ 235.66 (s), 196.96 (s), 151.41 (d), 133.72 (d), 130.41 (s), 129.37 (s), 128,56 (d), 126.92 (s), 118.51 (d), 105.64 (broad s), 73.93 (broad s), 25.66 (broad s), 18.00 (broad s) ppm. IR (CaF_2 window, THF, cm^{-1}) ν_{CO}: 1972, 1956.4, 1803. Anal. Calcd. for: $C_{33}H_{40}Ni_2O_3P_2$ (**12**) (%): C, 59.69; H, 6.07. Found: C, 59.61; H, 6.10.

Synthesis of Complex 12 from 1

Compound **1** (20 mg, 0.039 mmol, 1 equiv) and Ni(COD)$_2$ (21.2 mg, 0.077 mmol, 2 equiv) were transferred as a solution in *ca.* 5 mL of THF into a Schlenk tube fitted with a screw-in Teflon stopper along with a magnetic stirbar. The solution was stirred for *ca.* 20 minutes at room temperature during which time the solution turned deep red. The reaction mixture was then thoroughly degassed. The solution was cooled to -78 °C, and *ca.* 4 equivalents of CO were admitted using a calibrated gas bulb. The solution was then allowed to slowly warm to room temperature while stirring over 30 minutes during which time the color changed from red to orange and finally to pale yellow. The volatiles were then removed under reduced pressure. While complex **4** was found to be the majority product, a significant quantity of impurities of $P_2Ni_3(CO)_4$ as well as a transfacical polycarbonyl dinickel complex, with each phosphine coordinated to a $Ni(CO)_3$ or $Ni(CO)_2$ fragment, was observed which proved difficult to remove by recrystallization.[5g, 7a] Synthesis from complex **7** was therefore pursued as the predominant route to complex **12**.

Synthesis of Complex 10

Complex **9** (30.0 mg, 0.043 mmol, 1 equiv) was transferred as a solution in *ca.* 6 mL of THF to a 20 mL scintillation vial along with a magnetic stir bar. Ferrocenium hexafluorophosphate (14.5 mg, 0.043 mmol, 1 equiv) was then added as a solution in *ca.* 4 mL of THF. The reaction mixture was stirred for 30 minutes during which time the solution changed from red/orange to green/brown. The reaction mixture was then concentrated under reduced pressure, and *ca.* 5 mL of diethyl ether was added to precipitate out the product. The solid was washed with additional diethyl ether and then dissolved in minimal THF before filtering through a Celite pad and removing volatiles under reduced pressure. The emerald green residue was recrystallized by vapor diffusion of pentane into a concentrated THF solution at -35 °C to yield dark green crystalline needles. Complex **10** is *unstable* in THF solution and decomposes overnight at room temperature to ill-defined species. Complex **10** also immediately decomposes in acetonitrile. As a crystalline solid, complex **10** is indefinitely stable at room temperature. Yield: 14.7 mg (41 %). ^1H NMR (300 MHz, d_8-THF*)* shows no signals between 200 and -70 ppm, consistent with a paramagnetic compound with a weakly associated PF_6 counteranion. ^{31}P NMR (121 MHz*, d*$_8$-THF*)* shows no signals between 200 and -200 ppm, consistent with a paramagnetic compound with a weakly associated PF_6 counteranion. ^{19}F NMR (282 MHz, *d*$_8$-THF*)* shows a broadened doublet centered at -70.32 ppm, consistent with a weakly associated PF_6 counteranion. IR (ATR film, cm^{-1}) ν_{CO}: 2010, 1972, 1938, 1917. Anal. Calcd. for: $C_{34}H_{40}F_6Fe_2O_4P_3$ (**10**) (%): C, 49.13; H, 4.85. Found: C, 49.40; H, 4.85.

Synthesis of Complex 13-CO

A Schlenk tube fitted with a screw-in Teflon stopper was charged with 1,4-bis(2-diisopropylphosphino)phenyl)benzene (**1**) (500 mg, 1.08 mmol, 1 equiv) and Ni(COD)$_2$ (891.9 mg, 3.24 mmol, 3 equiv). THF (*ca.* 60 mL) was added and then the combined reaction mixture was degassed and sealed. After stirring for two hours a color change from yellow to dark red was observed. Following degassing the solution, the reaction mixture was cooled to -78°C and 5 equivalents of CO was admitted using a calibrated gas bulb. The reaction was allowed to slowly warm to room temperature while stirring. During this time the solution turned a bright red/orange. While stirring for an addition 16 h, the solution slowly turned yellow/brown, at which time volatiles were removed under reduced pressure to yield a yellow/brown residue. The residue was dissolved in minimal THF and filtered through a celite pad. The product was recrystallized from the filtrate by the slow vapor diffusion of hexanes over 3 days at room temperature to afford pure product as large dark crystals (37% yield). ^1H NMR (300 MHz, C_6D_6) δ 7.42 (d, 2H, aryl-*H*), 7.09-6.89 (m, 6H, aryl-*H*), 5.65 (s, 2H, central aryl-*H*), 4.57 (s, 2H, central aryl-*H*), 2.30 (m, 2H, C*H*), 2.12 (m, 2H, C*H*), 1.25 (dd, 6H, C*H*$_3$), 1.06 (dd, 12H, C*H*$_3$), 0.89 (dd, 6H, C*H*$_3$). ^{31}P NMR (121 MHz, C_6D_6) δ 50.32 (s). ^{13}C NMR (126 MHz, C_6D_6) δ 246.87 (s), 245.58 (s), 195.08 (s), 151.56 (m), 134.28 (m), 131.62 (s), 129.32 (s), 127.60 (s), 126.33 (s), 91.06 (s), 70.98 (s), 66.64 (s), 26.87 (m), 24.30 (m), 20.18 (s), 18.84 (s), 18.03 (t), 17.58 (s). IR (CaF_2 window, THF, cm^{-1}) ν_{CO}: 2002, 1873, 1830. Anal. Calcd. for: $C_{34}H_{40}Ni_3O_4P_2$ (**13-CO**) (%): C, 54.40; H, 5.37. Found: C, 54.31; H, 5.28.

Synthesis of Complex 13-PMe$_3$

In an inert atmosphere glovebox, a 20 mL scintillation vial was charged with **13-CO** (102 mg, 0.136 mmol, 1 equiv) and dissolved in THF (*ca.* 10 mL). While stirring, PMe_3 (1 M in THF, 149 μL, 1.1 equiv) was added via syringe. The reaction slowly turned from yellow to bright orange over the 16h reaction time. Volatiles were removed under reduced pressure to yield an orange residue. Pure product was obtained by the vapor diffusion of hexanes out of a concentrated hexanes/hexamethyldisiloxane solution to yield an orange precipitate (74% yield). ^{1}H NMR (300 MHz, C_6D_6) δ 7.71 (m, 2H, aryl-*H*), 7.07 (m, 4H, aryl-*H*), 6.94 (t, 2H, aryl-*H*), 5.13 (d, 2H, central aryl-*H*), 4.67 (d, 2H, central aryl-*H*), 2.41 (m, 2H, C*H*), 2.24 (m, 2H, C*H*), 1.38 (dd, 6H, C*H*$_3$), 1.16 (m, 12H, C*H*$_3$), 1.00 (d, 9H, C*H*$_3$), 0.99 (dd, 6H, C*H*$_3$). ^{31}P NMR (121 MHz, C_6D_6) δ 51.50 (d, *J* = 16.6 Hz), 6.61 (t, *J* = 16.6 Hz). ^{13}C NMR (126 MHz, C_6D_6) δ 259.93 (s), 250.72 (s), 153.21 (m), 135.345 (m), 131.55 (s), 128.87 (s), 127.26 (t), 125.74 (t), 88.31 (s), 68.17 (s), 63.15 (s), 27.01 (m), 24.47 (m), 20.45 (s), 19.11 (t), 18.29 (t), 17.82 (s), 14.48 (d). IR (CaF_2 window, C_6H_6, cm^{-1}) ν_{CO}: 1854, 1783. Anal. Calcd. for: $C_{36}H_{49}Ni_3O_3P_3$ (**6)** (%): C, 54.13; H, 6.18. Found: C, 54.44; H, 6.10.

Electrochemistry Details

Electrochemical measurements of complex **3**, **4**, **6**, **3-(OMe)$_2$**, **8**, **8-(OMe)$_2$**, and **9** were taken on a Pine Instrument Company biopotentiostat model AFCBP1 as 3 millimolar solutions in tetrahydrofuran using 0.1 molar [*n*Bu$_4$N][PF$_6$] as the electrolyte with a platinum wire counter electrode, a glassy carbon working electrode, and a silver/silver nitrate reference electrode in 0.1 molar [*n*Bu$_4$N][PF$_6$] as an acetonitrile solution. Electrochemical measurements of compounds were internally referenced to ferrocene.

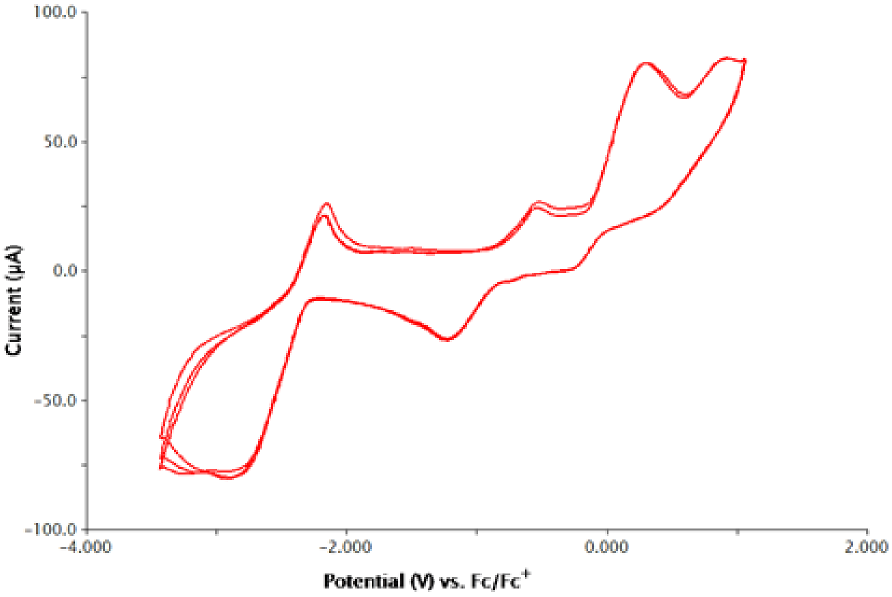

Figure 16. Complex **3** full cyclic voltammogram.

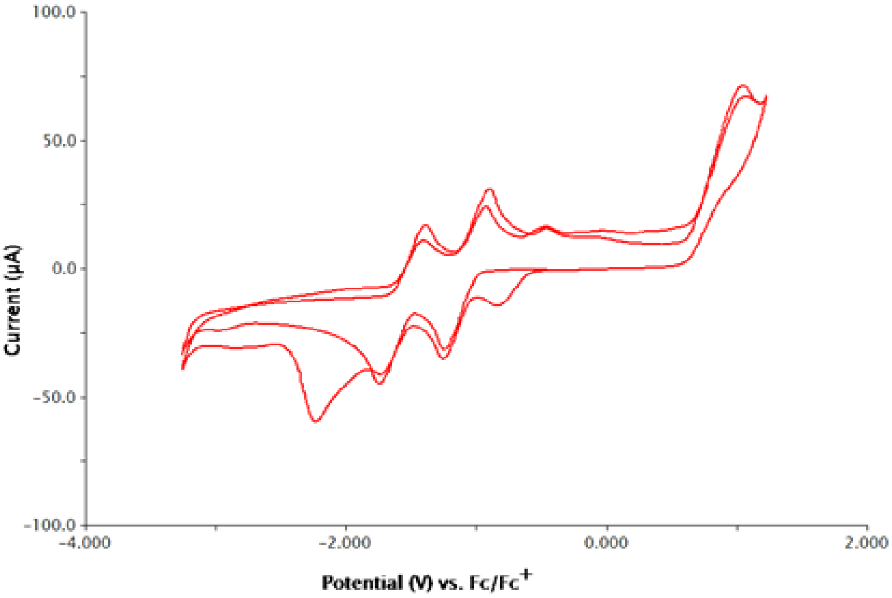

Figure 17. Complex **4** full cyclic voltammogram.

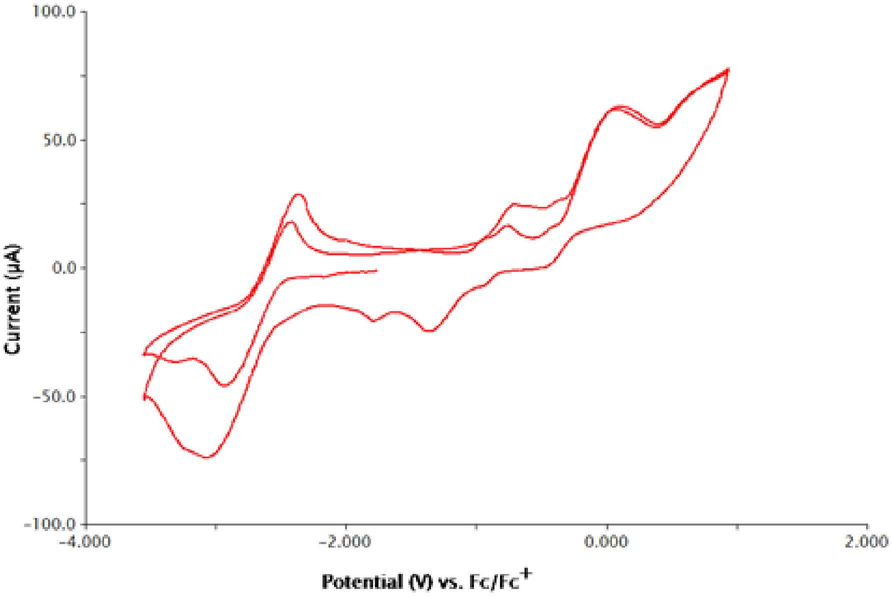

Figure 18. Complex **3-(OMe)$_2$** full cyclic voltammogram.

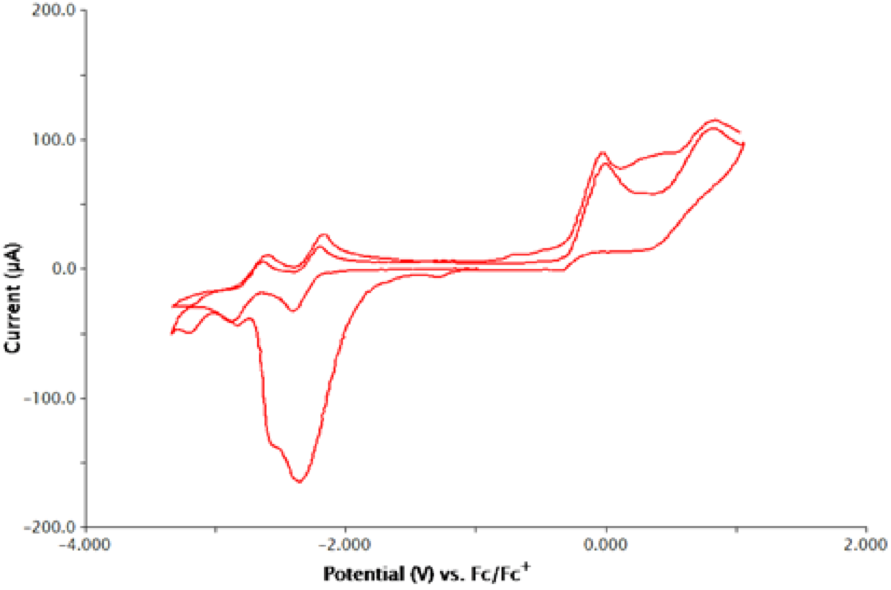

Figure S19. Complex **8** full cyclic voltammogram.

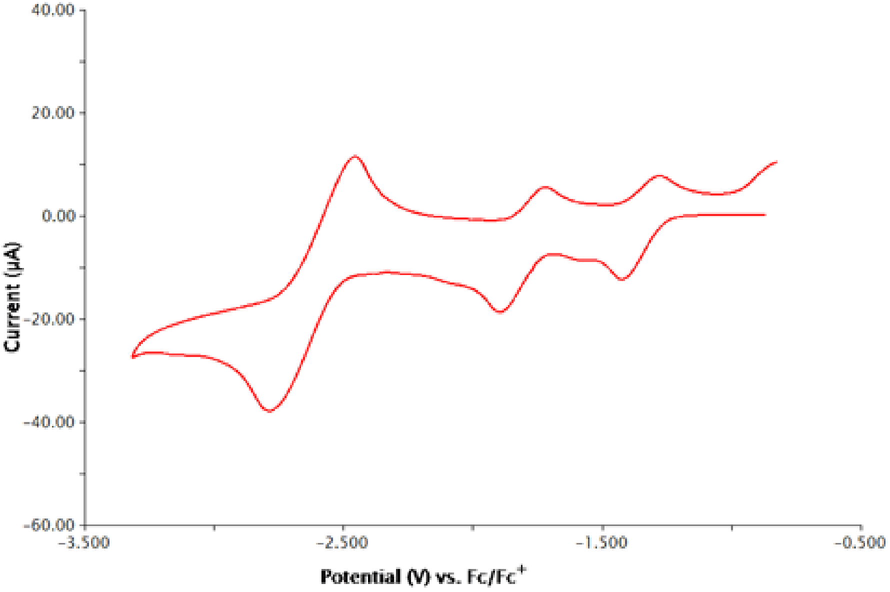

Figure 20. Complex **3-(OMe)$_2$** and **4** reductive scan as equimolar solution.

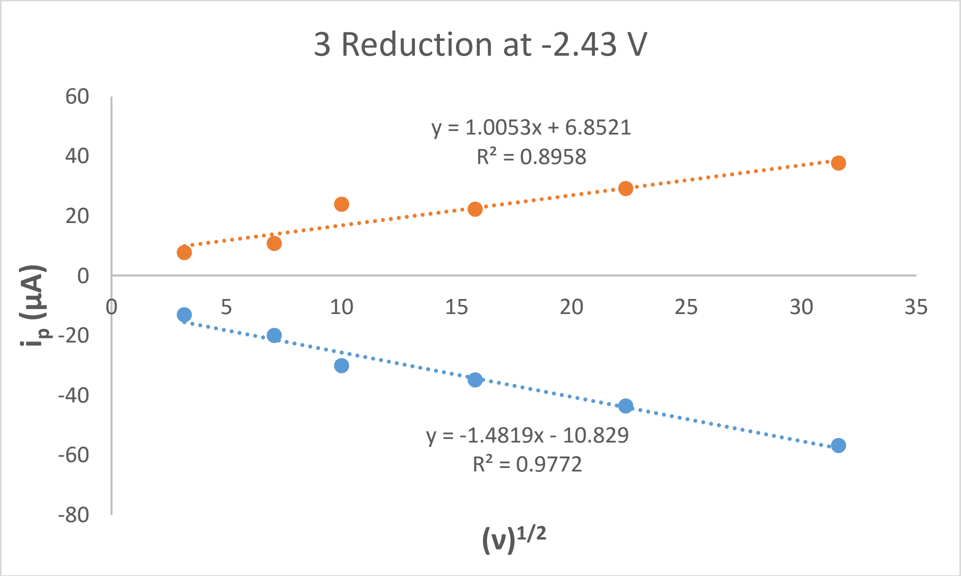

Figure 21. Plot of the scan rate dependence for the reduction of compound **3** with the cathodic (blue) and anodic scans (orange).

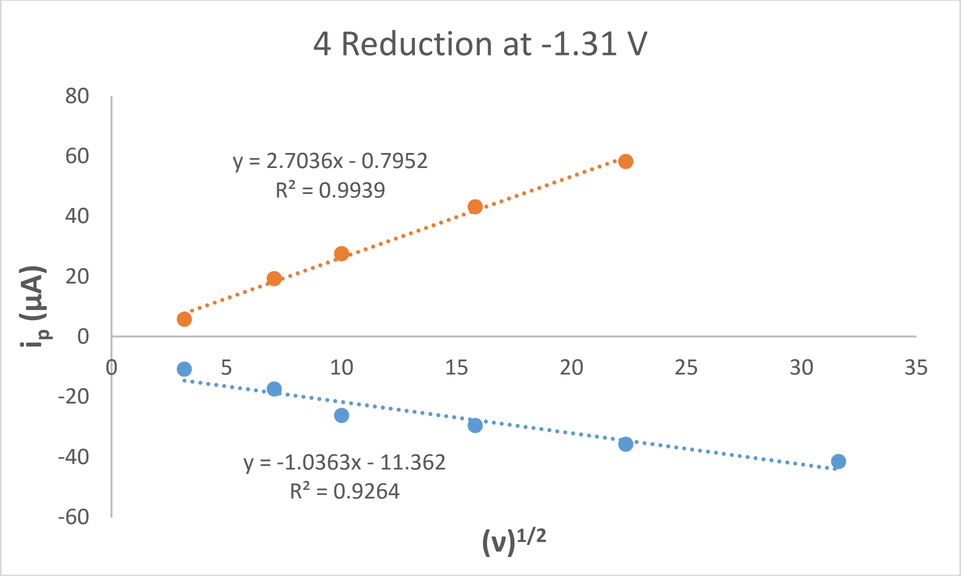

Figure 22. Plot of the scan rate dependence for the first reduction of compound **4** with the cathodic (blue) and anodic scans (orange).

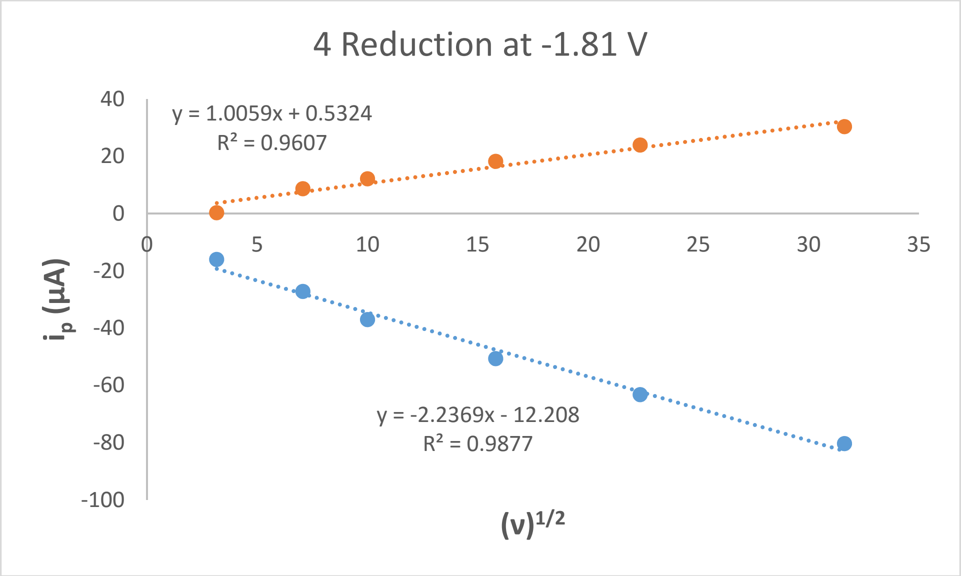

Figure 23. Plot of the scan rate dependence for the second reduction of compound **4** with the cathodic (blue) and anodic scans (orange).

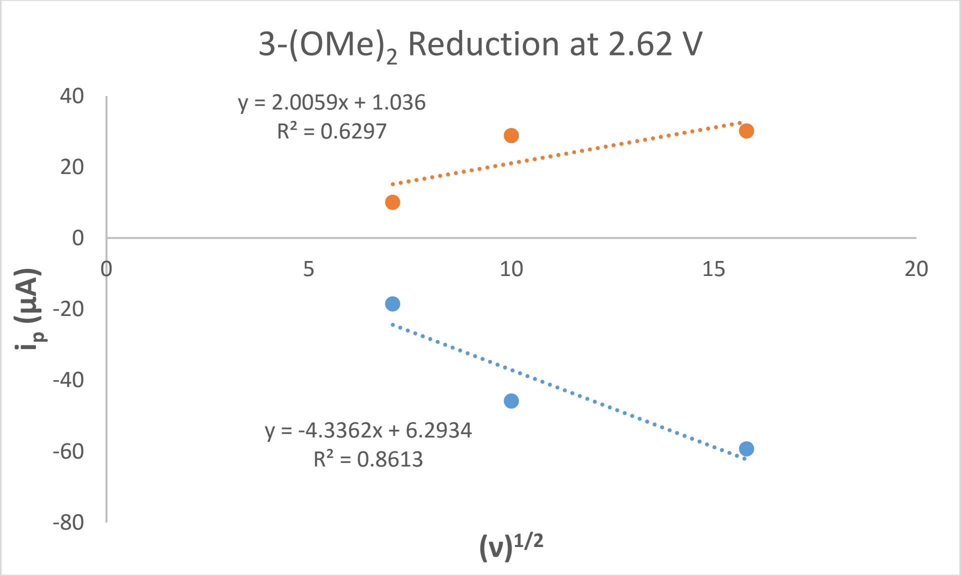

Figure 24. Plot of the scan rate dependence for the reduction of compound **3-(OMe)$_2$** with the cathodic (blue) and anodic scans (orange).

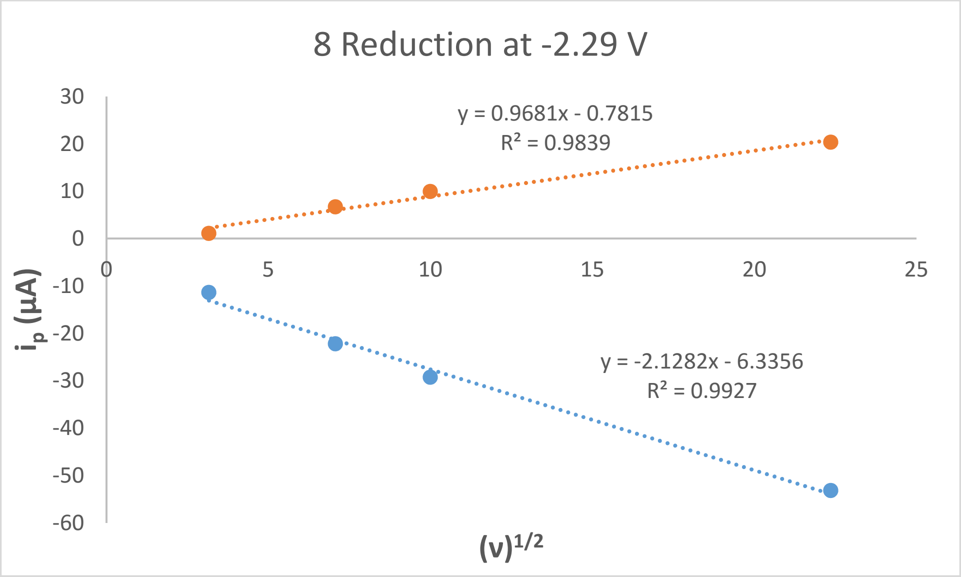

Figure 25. Plot of the scan rate dependence for the first reduction of compound **8** with the cathodic (blue) and anodic scans (orange).

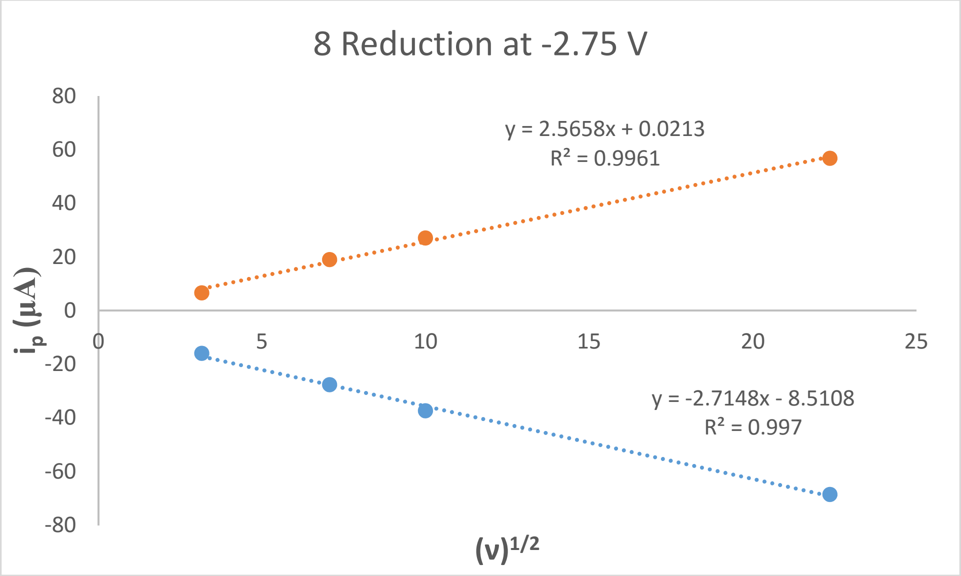

Figure 26. Plot of the scan rate dependence for the second reduction of compound **8** with the cathodic (blue) and anodic scans (orange).

Mössbauer Details

Spectra were recorded on a spectrometer from SEE Co. operating in the constant acceleration mode in a transmission geometry. Spectra were recorded with the temperature of the sample maintained at 80 K. The sample was kept in an SVT-400 Dewar from Janis, at zero field. Application of a magnetic field of 54 mT parallel to the γ-beam did not cause detectable changes in the spectra recorded at 80 K. The quoted isomer shifts are relative to the centroid of the spectrum of a metallic foil of α-Fe at room temperature. Samples were prepared by grinding polycrystalline material into a fine powder and then mounted in a cup fitted with a screw cap as a boron nitride pellet. Data analysis was performed using the program WMOSS (www. wmoss.org) and quadrupole doublets were fit to Lorentzian lineshapes.

Computational Details

All calculations were performed with DFT as implemented in Gaussian 09 Revision C.01.[29] Geometry optimizations and electronic structure calculations were performed with the TPSSh hybrid functional[30] that, incorporating 10% exact exchange (c.f. BLYP 0% and B3LYP 20%), has been shown to be effective for calculating transition metal-containing compounds.[31] The LANL2DZ basis set and effective core potential[32] for Pd atoms and the 6-31++G(d,p) basis set[33] for all other atoms was used. No solvent corrections were used. For all compounds isopropyl substituents on the phosphine ligands were truncated to methyl groups and have been designated with the -Me_2 suffix to the appropriate compound numbers. Geometry optimizations of **3-Me_2** and **3-$(OMe)_2$-Me_2** were performed under the C_2 point group, while **4-Me_2** and **8-Me_2** were optimized without symmetry constraints. Optimization stationary points were confirmed with subsequent frequency calculations that did not return imaginary frequency vibrations < -10 cm^{-1}. All molecular orbital illustrations are depicted with a 0.05 isosurface value. Natural bond order (NBO) calculations were performed to elucidate the nature of the M-M' interactions. There is an unresolved error with NBO3, as implemented in Gaussian09[8], when trying to do bonding analysis of these compounds. So to perform NBO bond analysis, the following procedure was used: the atomic coordinates from the Gaussian09 geometry optimizations were used to run single-point calculations in Orca (version 3.0.3[34]), and Orca was used to generate input files (*.47) for NBO6 [35] analysis. The NBO6 input files were modified by including the keywords BNDIDX and PLOT and listing analogous connectivity patterns in a $CHOOSE block before running. The natural localized molecular orbitals (NLMOs) were visualized using the pre-orthogonalized natural atomic orbitals basis set by opening the *.38 NBO6 output files with JMol.

Table 3. Select Molecular Orbital Illustrations for **3-Me$_2$**, **4-Me$_2$**, **3-(OMe)$_2$-Me$_2$**, and **8-Me$_2$**

3-Me$_2$	4-Me$_2$	3-(OMe)$_2$-Me$_2$	8-Me$_2$	Rep. MO
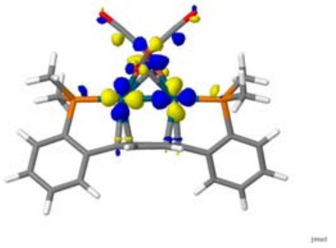 LUMO	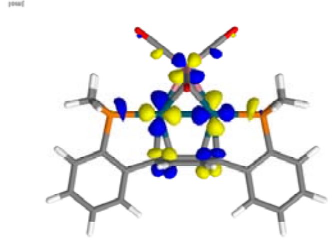 LUMO	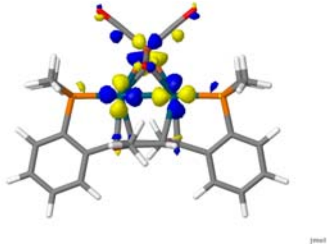 LUMO	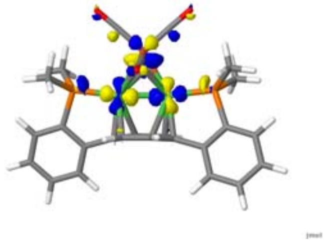 LUMO	M-M and M-M' antibonding
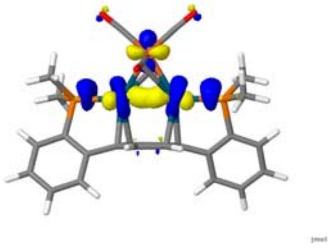 HOMO-2	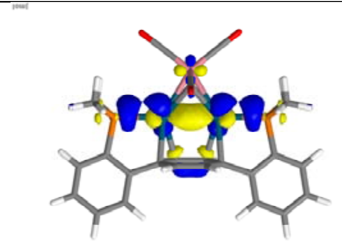 HOMO	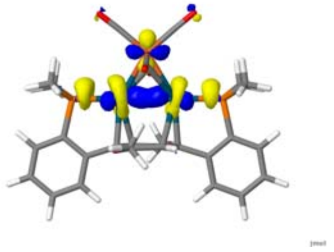 HOMO-2	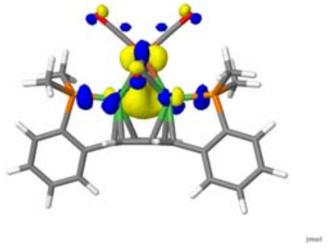 HOMO-1	M-M σ-bonding

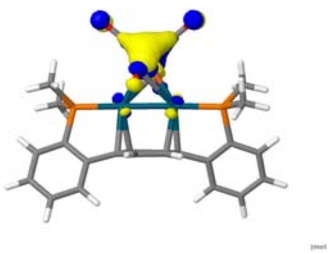 HOMO-4	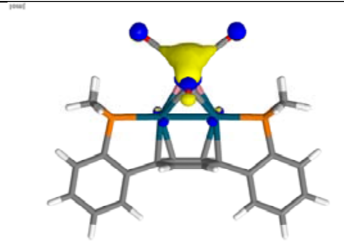 HOMO-5	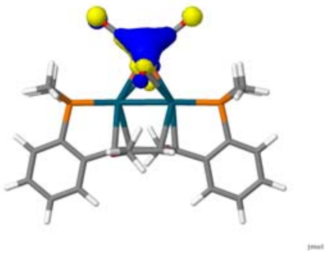 HOMO-4	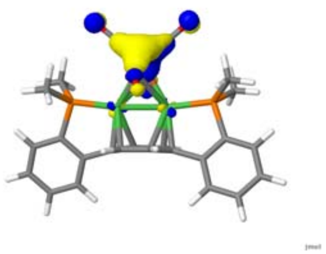 HOMO-4	M'-CO backbonding
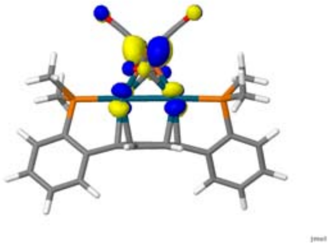 HOMO-5	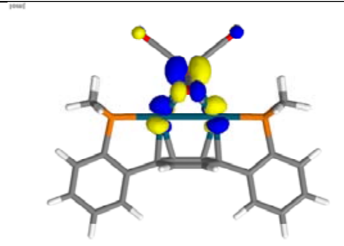 HOMO-16	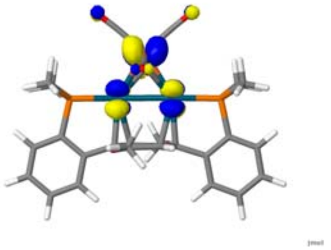 HOMO-5	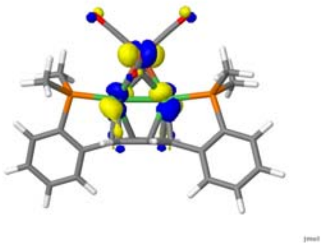 HOMO-7	M-M' π antibonding and M-M δ antibonding
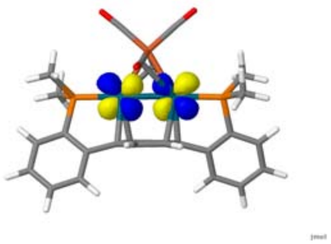 HOMO-10	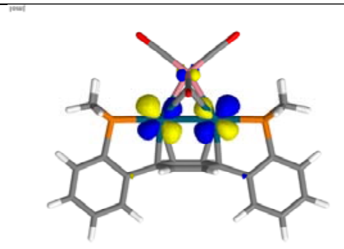 HOMO-13	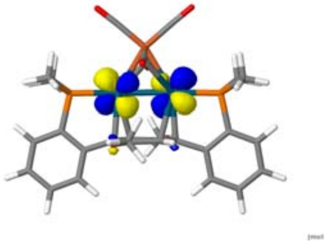 HOMO-10	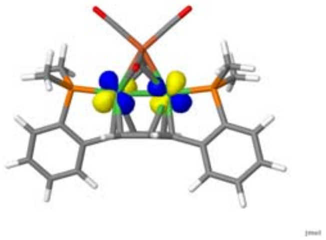 HOMO-9	M-M π-antibonding

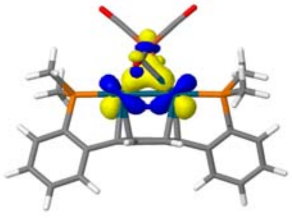 HOMO-17	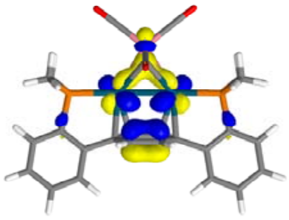 HOMO-18	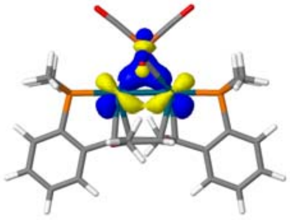 HOMO-18	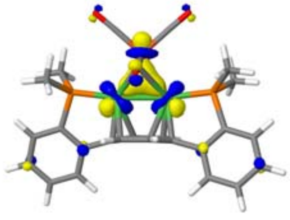 HOMO-17	M-M and M-M’ bonding
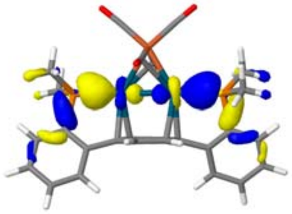 HOMO-19	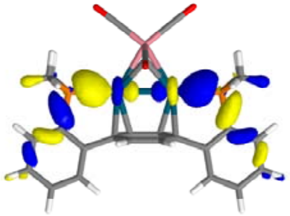 HOMO-17	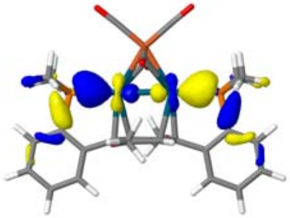 HOMO-20	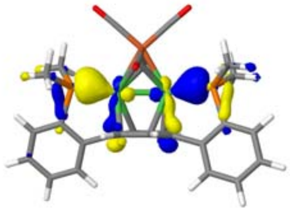 HOMO-18	M-P bonding
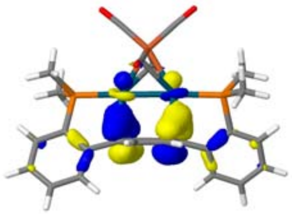 HOMO-20	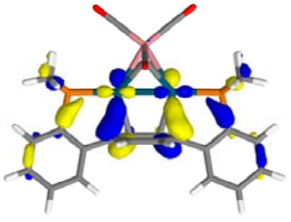 HOMO-23	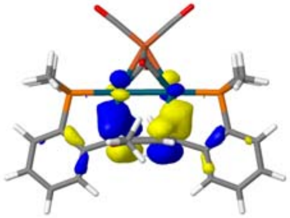 HOMO-21	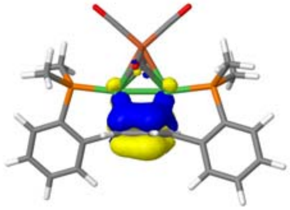 HOMO-19	M-arene bonding

3-Me$_2$ **4-Me$_2$** **3-(OMe)$_2$-Me$_2$** **78-Me$_2$**

62%, 62% 63%, 78% 70%, 64% 61%, 62%

Figure 27. a) Metal–metal and metal-CO Wiberg bond indices and b) (group 10 metal center)–(apical metal center) (M–M') natural localized molecular orbitals (NLMOs) and their contributions to total M–M' bond orders

Crystallographic Information

CCDC 1056167-1056171 contain the supplementary crystallographic data for the published compounds in Section 2.2. CCDC 981915, 737475, 981916, and 981917 contain the supplementary crystallographic data for the published complexes in Section 2.3. These data can be obtained free of charge from The Cambridge Crystallographic Data Centre via www.ccdc.cam.ac.uk/data_request/cif.

Refinement Details

In each case, crystals were mounted on a glass fiber or nylon loop using Paratone oil, then placed on the diffractometer under a nitrogen stream. Low temperature (100 K) X-ray data were obtained on a Bruker APEXII CCD based diffractometer (Mo sealed X-ray tube, K_α = 0.71073 Å). All diffractometer manipulations, including data collection, integration and scaling were carried out using the Bruker APEXII software.[36] Absorption corrections were applied using SADABS.[37] Space groups were determined on the basis of systematic absences and intensity statistics and the structures were solved by direct methods using XS (incorporated into SHELXTL) and refined by full-matrix least squares on F^2. All non-hydrogen atoms were refined using anisotropic displacement parameters. Hydrogen atoms were placed in idealized positions and refined using a riding model. The structure was refined (weighted least squares refinement on F^2) to convergence.

Special refinement details for 10

10 was crystallized from a THF-hexanes vapor diffusion at -35 ºC in an inert atmosphere glovebox. It was found to crystallize with a disordered THF solvent molecule with one oxygen modelled isotropically. The structure also contains an outer-sphere hexafluorophosphate anion that was satisfactorily modelled.

Table 4. Crystal and refinement data for complexes reported in Section 2.2

Complex	**3**	**4**	**5**	**6**	**3-(OMe)$_2$**	**8**
empirical formula	$C_{17}H_{20}Fe_{0.50}O_2PPd$	$C_{40}H_{47.50}BCoF_4N_{1.50}O_4P_2Pd_2$	$C_{34}H_{40}CoO_4P_2 Pd_2$	$C_{41}H_{52}B_2F_8MoN_4O_3P_2 Pd_2$	$C_{36}H_{44}FeO_6P_2 Pd_2$	$C_{17}H_{20}Fe_{0.50}NiO_2P$
formula wt	421.62	1033.77	846.33	1193.16	903.30	373.93
T (K)	100	100	100	100	100	100
a, Å	11.4622(6)	15.9326(8)	15.7355(5)	7.7570(7)	14.0587(5)	11.5996(6)
b, Å	13.3606(7)	16.5136(9)	13.6086(4)	15.4169(13)	14.2422(5)	13.1456(7)
c, Å	11.1153(5)	18.4384(10)	15.8392(5)	19.7029(18)	18.4208(6)	10.9589(5)
α, deg	90	90.490(3)	90	95.586(4)	90	90
β, deg	90	114.618(2)	90.1244(15)	91.721(4)	90	90
γ, deg	90	105.162(2)	90	95.546(4)	90	90
V, Å^3	1702.22(15)	4218.4(4)	3391.77(18)	2332.2(4)	3688.3(2)	1671.05(15)
Z	4	4	4	2	4	4
cryst syst	Orthorhombic	Triclinic	Monoclinic	Triclinic	Orthorhombic	Orthorhombic
space group	$P\ 2_1\ 2_1\ 2$	$P\ _{-1}$	P 1 21/n 1	P_{-1}	$P\ 2_1\ 2_1\ 2_1$	$P\ 2_1\ 2_1\ 2$
d_{calcd}, g/cm^3	1.645	1.628	1.657	1.699	1.627	1.486
θ range, deg	1.832 to 30.581	1.289 to 26.372	1.822 to 36.252	1.039 to 45.367	2.035 to 36.442	2.342 to 30.569
μ, mm^{-1}	1.595	1.367	1.662	1.170	1.482	1.675
abs cor	Semi-empirical from equivalents	Semi-empirical from equivalents	Semi-empirical from equivalents	Semi-empirical from equivalents	Semi-empirical from equivalents	Semi-empirical from equivalents
GOF[c]	1.172	1.077	1.175	1.042	1.070	1.082
R1,[a] wR2[b] (I > 2σ(I))	0.0142, 0.0352	0.0264, 0.0669	0.0378, 0.0791	0.0401, 0.1295	0.0325, 0.0638	0.0342, 0.0898

Table 5. Crystal and refinement data for complexes reported in Section 2.3

Complex	**9**	**11**	**12**	**10**	**13-CO**
empirical formula	$C_{34}H_{40}O_4P_2Fe_2$	$C_{39}H_{46}Co_2O_3P_2$	$C_{33}H_{40}Ni_2O_3P_2$	$C_{36}H_{44}F_6Fe_2O_{4.50}P_3$	$C_{34}H_{40}Ni_3O_4P_2$
formula wt	686.33	742.56	664.01	867.32	750.73
T (K)	100	100	100	100	100
a, Å	14.3107(5)	10.0645(4)	14.1146(4)	8.8633(4)	13.2747(6)
b, Å	11.4723(4)	11.1061(5)	15.1785(4)	15.6066(7)	14.3889(6)
c, Å	20.2029(7)	32.262(1)	15.6000(4)	27.166(1)	17.0160(7)
α, deg	90	90	90	90	90
β, deg	108.029(2)	91.975(2)	115.380(1)	98.310(2)	90
γ, deg	90	90	90	90	90
V, Å^3	3154.0(2)	3604.0(3)	3019.6(1)	3718.4(3)	3250.2(2)
Z	4	4	4	4	4
cryst syst	Monoclinic	Monoclinic	Monoclinic	Monoclinic	Orthorhombic
space group	$P2_1/c$	$P2_1/n$	$P2_1/c$	$P2_1/c$	$P2_12_12_1$
d_{calcd}, g/cm^3	1.4453	1.369	1.461	1.549	1.534
θ range, deg	3 to 73.66	1.94 to 36.81	1.972 to 30.656	2.000 to 30.598	1.85 to 37.24
μ, mm^{-1}	1.058	1.045	1.386	0.980	1.855
abs cor	Semi-empirical from equivalents	Semi-empirical from equivalents	Semi-empirical from equivalents	Semi-empirical from equivalents	Semi-empirical from equivalents
GOF^c	1.076	1.517	0.983	1.602	1.091
R1,^{a} wR2^b (I > 2σ(I))	0.0302, 0.1373	0.0373, 0.0624	0.0321, 0.1090	0.0267, 0.0732	0.0344, 0.0615

[a] $R1 = \Sigma||F_o|-|F_c|| / \Sigma|F_o|$ [b] $wR2 = \{ \Sigma [w(F_o^2-F_c^2)^2] / \Sigma [w(F_o^2)^2] \}^{1/2}$ [c] $GOF = S = \{ \Sigma [w(F_o^2-F_c^2)^2] / (n-p) \}^{1/2}$

EPR Details

Spectrum was collected on an X-band EPR (Frequency: 9.391 GHz; Power: 0.645 mW; Modulation Amplitude: 1 G) as a toluene glass at 77 K. EPR simulation run using EasySpin program for Matlab.[38] Simulation parameters: g = [2.128, 2.032, 1.930], lw = 2, HStrain = [20, 20, 20], Nucs = 'Co', A = [119 65 105].

REFERENCES

1.(a) Adams, R. D.; Cotton, F. A., *Catalysis by Di- and Polynuclear Metal Cluster Complexes.* Wiley-VCH: 1998; (b) Guczi, L., *Supported Bimetallic Catalysts Derived from Molecular Metal Complexes.* Elsevier Science Publishers B. V.: 1986; Vol. 29; (c) Braunstein, P.; Rosé, J., Heterometallic Clusters in Catalysis. In *Metal Clusters in Chemistry*, Braunstein, P.; Oro, L. A.; Raithby, P. R., Eds. Wiley-VCH: 1999.
2.Buchwalter, P.; Rosé, J.; Braunstein, P., *Chemical Reviews* **2015,** *115*, 28-126.
3.(a) Marquard, S. L.; Bezpalko, M. W.; Foxman, B. M.; Thomas, C. M., *J Am Chem Soc* **2013,** *135*, 6018-6021; (b) Krogman, J. P.; Foxman, B. M.; Thomas, C. M., *J Am Chem Soc* **2011,** *133*, 14582-14585; (c) Kuppuswamy, S.; Bezpalko, M. W.; Powers, T. M.; Wilding, M. J. T.; Brozek, C. K.; Foxman, B. M.; Thomas, C. M., *Chem. Sci.* **2014,** *5*, 1617-1626; (d) Napoline, J. W.; Krogman, J. P.; Shi, R.; Kuppuswamy, S.; Bezpalko, M. W.; Foxman, B. M.; Thomas, C. M., *Eur. J. Inorg. Chem.* **2013,** *2013*, 3874-3882; (e) Cooper, B. G.; Napoline, J. W.; Thomas, C. M., *Catal. Rev.* **2012,** *54*, 1-40; (f) Clouston, L. J.; Siedschlag, R. B.; Rudd, P. A.; Planas, N.; Hu, S. X.; Miller, A. D.; Gagliardi, L.; Lu, C. C., *J Am Chem Soc* **2013,** *135*, 13142-13148; (g) Rudd, P. A.; Liu, S. S.; Gagliardi, L.; Young, V. G.; Lu, C. C., *J Am Chem Soc* **2011,** *133*, 20724-20727; (h) Tereniak, S. J.; Carlson, R. K.; Clouston, L. J.; Young, V. G.; Bill, E.; Maurice, R.; Chen, Y. S.; Kim, H. J.; Gagliardi, L.; Lu, C. C., *J Am Chem Soc* **2014,** *136*, 1842-1855; (i) Banerjee, S.; Karunananda, M. K.; Bagherzadeh, S.; Jayarathne, U.; Parmelee, S. R.; Waldhart, G. W.; Mankad, N. P., *Inorganic Chemistry* **2014,** *53*, 11307-11315; (j) Collman, J. P.; Boulatov, R., *Angew. Chem. Int. Ed.* **2002,** *41*, 3948-3961.
4.(a) Jaouen, G.; Marinetti, A.; Mentzen, B.; Mutin, R.; Saillard, J. Y.; Sayer, B. G.; McGlinchey, M. J., *Organometallics* **1982,** *1*, 753-756; (b) Mlekuz, M.; Bougeard, P.; Sayer, B. G.; Peng, S.; McGlinchey, M. J.; Marinetti, A.; Saillard, J. Y.; Ben Naceur, J.; Mentzen, B.; Jaouen, G., *Organometallics* **1985,** *4*, 1123-1130; (c) Powers, T. M.; Gu, N. N. X.; Pout, A. R.; Baldwin, A. M.; Sanchez, R. H.; Alfonso, D. M.; Chen, Y. S.; Zheng, S. L.; Betley, T. A., *J Am Chem Soc* **2013,** *135*, 14448-14458; (d) Eames, E. V.; Sanchez, R. H.; Betley, T. A., *Inorganic Chemistry* **2013,** *52*, 5006-5012; (e) Braunstein, P.; Sappa, E.; Tiripicchio, A.; Camellini, M. T., *Inorganica Chimica Acta* **1980,** *45*, L191-L193; (f) Sironi, A.; Gervasio, G.; Sappa, E., *Journal of Cluster Science* **1994,** *5*, 535-548; (g) Bachert, I.; Braunstein, P.; McCart, M. K.; Biani, F. F. d.; Laschi, F.; Zanello, P.; Kickelbick, G.; Schubert, U., *Journal of Organometallic Chemistry* **1999,** *573*, 47-59; (h) Braunstein, P.; Ries, M.; Bellefon, C. d. M. d., *Journal of Organometallic Chemistry* **1988,** *355*, 533-550; (i) Braunstein, P.; Bellefon, C. d. M. d.; Ries, M.;

Fischer, J.; Bouaoud, S.-E.; Grandjean, D., *Inorganic Chemistry* **1988,** *27*, 1327-1337; (j) Braunstein, P.; Guarino, N.; de Méric de Bellefon, C.; Richert, J.-L., *Angewandte Chemie International Edition in English* **1987,** *26*, 88-89; (k) Archambault, C.; Bender, R.; Braunstein, P.; Bouaoud, S.-E.; Rouag, D.; Golhen, S.; Ouahab, L., *Chemical Communications* **2001**, 849-850; (l) Sappa, E.; Tiripicchio, A.; Braunstein, P., *Chemical Reviews* **1983,** *83*, 203-239; (m) Sappa, E.; Tiripicchio, A.; Braunstein, P., *Coordination Chemistry Reviews* **1985,** *65*, 219-284; (n) Braunstein, P.; De Meric de Bellefon, C.; Ries, M., *Inorganic Chemistry* **1990,** *29*, 1181-1186; (o) Lal De, R.; Von Seyerl, J.; Huttner, G., *Journal of Organometallic Chemistry* **1979,** *178*, 319-324; (p) Bender, R.; Braunstein, P.; Metz, B.; Lemoine, P., *Organometallics* **1984,** *3*, 381-384; (q) Vahrenkamp, H., *Pure Appl Chem* **1991,** *63*, 643-649; (r) Barr, R. D.; Green, M.; Howard, J. A. K.; Marder, T. B.; Stone, F. G. A., *J Chem Soc Chem Comm* **1983**, 759-760; (s) Carriedo, G. A.; Howard, J. A. K.; Stone, F. G. A., *Journal of Organometallic Chemistry* **1983,** *250*, C28-C32.
5.(a) Tard, C.; Pickett, C. J., *Chemical Reviews* **2009,** *109*, 2245-2274; (b) Gloaguen, F.; Rauchfuss, T. B., *Chem Soc Rev* **2009,** *38*, 100-108; (c) Darensbourg, M. Y.; Lyon, E. J.; Smee, J. J., *Coordination Chemistry Reviews* **2000,** *206*, 533-561; (d) Camara, J. M.; Rauchfuss, T. B., *Nat Chem* **2012,** *4*, 26-30; (e) Shibata, T., *Adv Synth Catal* **2006,** *348*, 2328-2336; (f) Mazzoni, R.; Salmi, M.; Zanotti, V., *Chem-Eur J* **2012,** *18*, 10174-10194; (g) Velian, A.; Lin, S.; Miller, A. J. M.; Day, M. W.; Agapie, T., *J. Am. Chem. Soc.* **2010,** *132*, 6296-6297; (h) Beck, R.; Johnson, S. A., *Chemical Communications* **2011,** *47*, 9233-9235; (i) Laskowski, C. A.; Hillhouse, G. L., *Chem. Sci.* **2011,** *2*, 321-325; (j) Laskowski, C. A.; Hillhouse, G. L., *Organometallics* **2009,** *28*, 6114-6120; (k) Delaet, D. L.; Delrosario, R.; Fanwick, P. E.; Kubiak, C. P., *J Am Chem Soc* **1987,** *109*, 754-758; (l) Lee, C. H.; Laitar, D. S.; Mueller, P.; Sadighi, J. P., *J Am Chem Soc* **2007,** *129*, 13802-13803; (m) Simon-Manso, E.; Kubiak, C. P., *Organometallics* **2005,** *24*, 96-102; (n) Lemke, F. R.; Delaet, D. L.; Gao, J. L.; Kubiak, C. P., *J Am Chem Soc* **1988,** *110*, 6904-6906; (o) Friedle, S.; Reisner, E.; Lippard, S. J., *Chem Soc Rev* **2010,** *39*, 2768-2779; (p) Ritleng, V.; Chetcuti, M. J., *Chemical Reviews* **2007,** *107*, 797-858; (q) Haak, R. M.; Wezenberg, S. J.; Kleij, A. W., *Chemical Communications* **2010,** *46*, 2713-2723; (r) Wheatley, N.; Kalck, P., *Chemical Reviews* **1999,** *99*, 3379-3419.
6.Gavrilova, A. L.; Bosnich, B., *Chemical Reviews* **2004,** *104*, 349-383.
7.(a) Suseno, S.; Horak, K. T.; Day, M. W.; Agapie, T., *Organometallics* **2013,** *32*, 6883-6886; (b) Lin, S.; Herbert, D. E.; Velian, A.; Day, M. W.; Agapie, T., *JACS* **2013,** *135*, 15830-15840; (c) Chao, S. T.; Lara, N. C.; Lin, S.; Day, M. W.; Agapie, T., *Angew. Chem. Int. Ed.* **2011,** *50*, 7529-7532.
8.Velian, A.; Lin, S. B.; Miller, A. J. M.; Day, M. W.; Agapie, T., *J Am Chem Soc* **2010,** *132*, 6296-6297.
9.Kelley, P.; Lin, S.; Edouard, G.; Day, M. W.; Agapie, T., *J Am Chem Soc* **2012,** *134*, 5480-5483.
10.(a) Lin, S. B.; Herbert, D. E.; Velian, A.; Day, M. W.; Agapie, T., *J Am Chem Soc* **2013,** *135*, 15830-15840; (b) Chao, S. T.; Lara, N. C.; Lin, S. B.; Day, M. W.; Agapie, T., *Angew. Chem. Int. Ed.* **2011,** *50*, 7529-7532; (c) Horak, K. T.; Velian, A.; Day, M. W.; Agapie, T., *Chemical Communications* **2014,** *50*, 4427-4429.
11.(a) Murahashi, T.; Takase, K.; Oka, M.-a.; Ogoshi, S., *J Am Chem Soc* **2011,** *133*, 14908-14911; (b) Ishikawa, Y.; Kimura, S.; Takase, K.; Yamamoto, K.; Kurashige, Y.; Yanai, T.; Murahashi, T., *Angewandte Chemie International Edition* **2015,** *54*, 2482-2486.
12.(a) Cristiani, F.; De Filippo, D.; Deplano, P.; Devillanova, F.; Diaz, A.; Trogu, E. F.; Verani, G., *Inorganica Chimica Acta* **1975,** *12*, 119-122; (b) Siclovan, O. P.; Angelici, R. J., *Inorganic Chemistry* **1998,** *37*, 432-444.

13.Bender, R.; Braunstein, P.; Bouaoud, S.-E.; Rouag, D.; Harvey, P. D.; Golhen, S.; Ouahab, L., *Inorganic Chemistry* **2002,** *41*, 1739-1746.

14.(a) Aguirre-Etcheverry, P.; Ashley, A. E.; Balazs, G.; Green, J. C.; Cowley, A. R.; Thompson, A. L.; O'Hare, D., *Organometallics* **2010,** *29*, 5847-5858; (b) Kerber, R. C.; Miran, M. J.; Waldbaum, B.; Rheingold, A. L., *Organometallics* **1995,** *14*, 2002-2008; (c) Putnik, C. F.; Welter, J. J.; Stucky, G. D.; D'Aniello Jr., M. J.; Sosinsky, B. A.; Kirner, J. F.; Muetterties, E. L., *JACS* **1978,** *100*, 4107-4116; (d) Knox, S. A. R.; Morton, D. A. V.; Orpen, A. G.; Turner, M. L., *Inorganica Chimica Acta* **1994,** *220*, 201-214.

15.(a) Lu, C. C.; Saouma, C. T.; Day, M. W.; Peters, J. C., *J Am Chem Soc* **2007,** *129*, 4-5; (b) Schneider, J. J.; Specht, U.; Goddard, R.; Krüger, C.; Ensling, J.; Gütlich, P., *Chem. Ber.* **1995,** *128*, 941-945; (c) Jonas, K.; Koepe, G.; Schieferstein, L.; Mynott, R.; Kruger, C.; Tsay, Y. H., *Angew. Chem. Int. Ed. Engl.* **1983,** *22*, 620-621.

16.A CSD search of dinuclear Co or Fe complexes bound to a cyclic C6-fragment yielded 1 cofacial and 1 transfacial Fe2 complex and 1 transfacial Co2 complex with a μ2:(η3,η3) binding mode.

17.Casati, N.; Macchi, P.; Sironi, A., *Angew. Chem. Int. Ed.* **2005,** *44*, 7736-7739.

18.(a) Johnson, S. A.; Taylor, E. T.; Cruise, S. J., *Organometallics* **2009,** *28*, 3842-3855; (b) Bach, I.; Porschke, K. R.; Goddard, R.; Kopiske, C.; Kruger, C.; Rufinska, A.; Seevogel, K., *Organometallics* **1996,** *15*, 4959-4966.

19.(a) Mezailles, N.; LeFloch, P.; Waschbusch, K.; Ricard, L.; Mathey, F.; Kubiak, C. P., *Journal of Organometallic Chemistry* **1997,** *541*, 277-283; (b) Osborn, J. A.; Stanley, G. G., *Angew Chem Int Edit* **1980,** *19*, 1025-1026.

20.Liu, T. B.; Darensbourg, M. Y., *J Am Chem Soc* **2007,** *129*, 7008-7009.

21.(a) Osborn, J. A.; Stanley, G. G.; Bird, P. H., *J Am Chem Soc* **1988,** *110*, 2117-2122; (b) Vogl, E. M.; Bruckmann, J.; Kruger, C.; Haenel, M. W., *Journal of Organometallic Chemistry* **1996,** *520*, 249-252.

22.(a) Munha, R. F.; Zarkesh, R. A.; Heyduk, A. F., *Dalton T* **2013,** *42*, 3751-3766; (b) Luca, O. R.; Crabtree, R. H., *Chem Soc Rev* **2013,** *42*, 1440-1459; (c) Annibale, V. T.; Song, D. T., *Rsc Adv* **2013,** *3*, 11432-11449; (d) Eisenberg, R.; Gray, H. B., *Inorganic Chemistry* **2011,** *50*, 9741-9751; (e) Chirik, P. J.; Wieghardt, K., *Science* **2010,** *327*, 794-795.

23.Pangborn, A. B.; Giardello, M. A.; Grubbs, R. H.; Rosen, R. K.; Timmers, F. J., *Organometallics* **1996,** *15*, 1518-1520.

24.Zhao, Y. L.; Liu, L. H.; Zhang, W. Y.; Sue, C. H.; Li, Q. W.; Miljanic, O. S.; Yaghi, O. M.; Stoddart, J. F., *Chem-Eur J* **2009,** *15*, 13356-13380.

25.Murahashi, T.; Nagai, T.; Okuno, T.; Matsutani, T.; Kurosawa, H., *Chemical Communications* **2000**, 1689-1690.

26.Edgell, W. F.; Lyford, J., *Inorganic Chemistry* **1970,** *9*, 1932-1933.

27.Strong, H.; Krusic, P. J.; San Filippo, J., *Inorganic Syntheses.* 1986; Vol. 24.

28.Fulmer, G. R.; Miller, A. J. M.; Sherden, N. H.; Gottlieb, H. E.; Nudelman, A.; Stoltz, B. M.; Bercaw, J. E.; Goldberg, K. I., *Organometallics* **2010,** *29*, 2176-2179.

29.1) Gaussian 09, Revision C.01, Frisch, M. J.; Trucks, G. W.; Schlegel, H. B.; Scuseria, G. E.; Robb, M. A.; Cheeseman, J. R.; Scalmani, G.; Barone, V.; Mennucci, B.; Petersson, G. A.; Nakatsuji, H.; Caricato, M.; Li, X.; Hratchian, H. P.; Izmaylov, A. F.; Bloino, J.; Zheng, G.; Sonnenberg, J. L.; Hada, M.; Ehara, M.; Toyota, K.; Fukuda, R.; Hasegawa, J.; Ishida, M.; Nakajima, T.; Honda, Y.; Kitao, O.; Nakai, H.; Vreven, T.; Montgomery, Jr., J. A.; Peralta, J. E.; Ogliaro, F.; Bearpark, M.; Heyd, J. J.; Brothers, E.; Kudin, K. N.; Staroverov, V. N.; Kobayashi, R.; Normand, J.; Raghavachari, K.; Rendell, A.; Burant, J. C.; Iyengar, S. S.; Tomasi, J.; Cossi, M.; Rega, N.; Millam, J. M.; Klene, M.; Knox, J. E.; Cross, J. B.; Bakken, V.; Adamo, C.; Jaramillo, J.; Gomperts, R.; Stratmann, R. E.; Yazyev, O.; Austin, A. J.; Cammi, R.; Pomelli, C.; Ochterski, J. W.; Martin, R. L.; Morokuma, K.; Zakrzewski, V. G.; Voth, G. A.; Salvador, P.; Dannenberg, J. J.; Dapprich, S.; Daniels, A. D.; Farkas, Ö.; Foresman, J. B.; Ortiz, J. V.; Cioslowski, J.; Fox, D. J. Gaussian, Inc., Wallingford CT, 2009.

30.(a) Tao, J. M.; Perdew, J. P.; Staroverov, V. N.; Scuseria, G. E., *Phys. Rev. Lett.* **2003,** *91*; (b) Staroverov, V. N.; Scuseria, G. E.; Tao, J. M.; Perdew, J. P., *J. Chem. Phys.* **2003,** *119*, 12129-12137.

31.(a) Jensen, K. P., *Inorganic Chemistry* **2008,** *47*, 10357-10365; (b) Buhl, M.; Kabrede, H., *J. Chem. Theory Comput.* **2006,** *2*, 1282-1290; (c) Waller, M. P.; Braun, H.; Hojdis, N.; Buhl, M., *J. Chem. Theory Comput.* **2007,** *3*, 2234-2242.

32.Hay, P. J.; Wadt, W. R., *J. Chem. Phys.* **1985,** *82*, 270-283.

33.Ditchfield, R.; Hehre, W. J.; Pople, J. A., *J. Chem. Phys.* **1971,** *54*, 724-728.

34.Neese, F., Wiley Interdiscip. Rev.: Comput. Mol. Sci., 2012, 2, 73-78.

35.NBO 6.0. Glendening, E. D., Badenhoop, J. K., Reed, A. E., Carpenter, J. E., Bohmann, J. A., Morales, C. M., Landis, C. R., Weinhold, F. (Theoretical Chemistry Institute, University of Wisconsin, Madison, WI, 2013), http://nbo6.chem.wisc.edu/

36.APEX2, Version 2 User Manual, M86-E01078, Bruker Analytical X-ray Systems, Madison, WI, June 2006.

37.Sheldrick, G. M. "SADABS (Version 2008/1): Program for Absorption Correction for Data from Area Detector Frames", University of Göttingen, 2008.

38.Stoll, S.; Schweiger, A., *J Magn Reson* **2006,** *178*, 42-55.